LABPLAS

Horizon 2020
European Union Funding
for Research & Innovation

Land-Based Solutions for Plastics in the Sea

This project has received funding from the European Union's Horizon 2020 research and innovation programme under grant agreement No 101003954

D7.4 Description of the process-based sea dispersal model

Due date of deliverable: 31/05/2024

Actual submission date: 31/05/2024

Horizon 2020
European Union Funding
for Research & Innovation

LABPLAS

Horizon 2020
European Union Funding
for Research & Innovation

PROJECT INFORMATION

Project number: 101003954

Project acronym: LABPLAS

Project full title: Land-Based Solutions for Plastics in the Sea

Call: H2020-SC5-2018-2019-2020 submitted for H2020-SC5-2020-2 / 03 Sep 2020

Topic: CE-SC5-30-2020 – Plastics in the environment: understanding the sources, transport, distribution and impacts of plastics pollution

Type of action: RIA – Research and Innovation Action

Starting date: June 1st, 2021

Duration: 48 months

List of participants:

Nº	Participant name	Acronym	Country	Type
1	UNIVERSIDADE DE VIGO	UVI	SPAIN	HES
2	UNIVERSIDADE DA CORUÑA	UDC	SPAIN	HES
3	BUNDESANSTALT FUER GEWAESSERKUNDE	BfG	GERMANY	RTO
4	LABORATORIO IBERICO INTERNACIONAL DE NANOTECNOLOGIA	INL	PORTUGAL	RTO
5	KATHOLIEKE UNIVERSITEIT LEUVEN	KUL	BELGIUM	HES
6	HELMHOLTZ ZENTRUM FUR OZEANFORSCHUNG KIEL	GEOMAR	GERMANY	RTO
7	NATIONAL OCEANOGRAPHY CENTRE	NOC	UNITED KINGDOM	RTO
8	SORBONNE UNIVERSITE	SU	FRANCE	HES
9	OPEN UNIVERSITEIT NEDERLAND	OUNL	NETHERLANDS	HES
10	LEIBNIZ INSTITUTE FOR BALTIC SEA RESEARCH	IOW	GERMANY	RTO
11	ASSOCIACAO PARA O DESENVOLVIMENTO DO ATLANTIC INTERNATIONAL RESEARCH CENTRE	AC	PORTUGAL	RTO
12	UNIVERSIDADE FEDERAL DO SAO PAULO	UNIFESP	BRASIL	HES
13	BASF SE	BASF	GERMANY	LE
14	TG ENVIRONMENTAL RESEARCH	ER	UNITED KINGDOM	SME
15	CONTACTICA S.L.	CTA	SPAIN	SME
16	STICHTING EGI	EGI	NETHERLANDS	Non-P
17	STICHTING RADBOUD UNIVERSITEIT	RU	NETHERLANDS	HES
18	UNIVERSIDADE FEDERAL DO PARÁ	UFPA	BRASIL	HES

DELIVERABLE DETAILS

Document number:	D 7.4
Document title:	D7.4 Description of the process-based sea dispersal model
Dissemination level	OA - Public
Period:	PR1 – PR2 – PR3
WP:	WP7
Task:	Task 7.3
Status:	Final
Author:	KU LEUVEN
Reviewers:	
Recommended citation format	Toorman, E.A., Gineau, A., Shettigar, N.A., Riom, W., 2024, Description of the process-based sea dispersal model. Technical Report, Deliverable 7.4, LABPLAS Grant Agreement No. 101003954 H2020-SC5-2020-2
Executive summary:	This report corresponds to deliverable 7.4 which describes the process based plastic litter sea dispersal model of the WP 7 Modelling, task 7.3 – Description of the 3D particle dispersal model for the North Sea, set-up in the open-source TELEMAC suite, including the model domain, the computational grid, the modules used with the processes considered and equations solved, and the methodology and data sources for set-up, initialization, boundary conditions, calibration and validation of the entire model.

Version	Date	Comments
1.0	30/04/2024	This deliverable 7.4 describes the model methodology and structure, while the final model setup and the model results will be integrated into the deliverable 7.3.

Disclaimer

The views and opinions expressed in this document reflect only the authors' views, and not necessarily those of the European Commission.

TABLE OF CONTENTS

LIST OF FIGURES

ABBREVIATIONS & ACRONYMS

Acronym	Description
MP	microplastics
DC	Discrete Classes
PBE	Population Balance Method
3D	3 dimensional
CPU	Central Processing Unit
CFD	Computational Fluid Dynamic

1 INTRODUCTION

Plastic pollution in oceans and rivers has become a serious concern, fearing to develop into an environmental threat to ecosystems, aquatic life and human health (Rochman *et al.*, 2016, Gall & Thompson, 2015) while the global plastic production keeps growing exponentially. Without improvements to its life cycle, an estimated 12 billion Mt of plastic litter may end up in landfills and in the natural environment by 2050 (² *et al.* 2017).

Many studies have attempted to quantify plastic dispersal into the environment on a global scale. However, there remains a big knowledge gap to explain the discrepancy between the estimated amounts entering the environment, typically obtained using a Mass Flow Analysis (MFA), and the much lower amounts found in the aquatic environment. Many hypotheses have been put forward, but it remains very difficult to find proof. An important gap, rarely addressed, is the estimation of the fraction of the MFA calculated amounts which reach the rivers, along which pathway, the source locations and source strengths.

Computer simulations, solving numerically the basic conservation equations for particles and the transporting medium (water and air) is theoretically the most accurate methodology to allows a physics-based description of the system. Because of the complexity, the high computational costs and the huge data needs, this approach is not often taken, as it also requires a lot of knowledge, experience and skill. Most modelling attempts applied to the aquatic plastic litter dispersal, documented in the literature, have oversimplified the system, which does not allow to take into account all physics, which are all interacting. This may lead to wrong interpretations and conclusions.

Within the LABPLAS project, the KU Leuven is applying their experience in coastal and estuarine sediment transport modelling to plastic particles. Their research task in WP7 consists of two-dimensional depth-averaged horizontal (2DH) of a selected river, i.e. the Elbe as one of the best documented systems in the current project, and full three-dimensional (3D) modelling of the North Sea. Both models interact, as the Elbe model requires open-sea boundary data, while the North Sea model needs input loads of sediment and plastic particles coming from land via the river.

This deliverable provides a description of the 3D dispersal model for the North Sea, to be validated with data from the LABPLAS field campaigns (WP2), processed in WP3, and complemented with available data from other projects. The aim is to clarify the structure of the model in terms of processes described, the numerical implementation and the data needed.

As the 2DH river and 3D North Sea model need to be linked to attempt to answer the question on the mechanisms through which plastics are dispersed in both the horizontal plane and over the depth, the model results of the 3D model will be discussed together with those of the 2DH river model in the final deliverable D7.3.

1.1 Aim of the 3D model

The 3D model attempts to give new insights into the distribution and pathways of plastic litter entering the North Sea from riverine influxes and local sources (remobilization of historical pollution on shorelines and the sea bottom, and garbage from ships and offshore structures).

Why a 3D model?

Since the density of many plastic polymers is close to the one of water, it is important to consider variations of both temperature and salinity fields which significantly impact the water density. Subsequently, density changes in water can induce additional gravity driven currents.

Temperature variations have different origins. The sea surface temperature is regulated by heat exchange with the atmosphere, which can be amplified due to wind. The sea bottom temperature is regulated by heat exchange with the earth beneath. The temperature of river water often differs from the seawater temperature. Ocean currents passing through the area may on their turn import water with different temperatures.

Also, salinity typically changes from freshwater inland, over brackish water in estuaries to partially saline water at the coast and to fully saline seawater offshore, i.e. going from 0 to over 30 ppm, and increase in density of the order of 3%. Since salt water is heavier, it is possible that the flood will penetrate an estuary over the bottom when a strong river outflow may keep the freshwater flowing downstream at the surface. This is a stratified condition. River discharges in European rivers usually are not so strong. In such cases the two layers will get mixed over the water column and only horizontal salinity gradients might be considered.

Moreover, the variation of temperature and salinity also impact water viscosity. The sensitivity of the value of the viscosity to temperature and salinity is much higher than that of the density. Both parameters play an important role in the determination of the drag force on particles. This becomes crucial in the estimation of the particle settling velocity under the external gravity force field, as presented in section 2.1.

These considerations on water property dependencies result in complex 3D interactions between water currents and the dynamics of plastic litter. Such complex interactions can only be captured thanks to 3D simulations of the coupled hydrodynamic and plastic transport fields.

The North Sea is known to be affected by all of these processes. Therefore, it is believed that it is necessary to take these 3D aspects into account to better understand the occurrences of plastic litter in the water column and at the sea bottom.

1.2 Principles of numerical modelling

Modelling the North Sea hydrodynamic, coupled with the dynamics of plastic litter, is conducted with the numerical solver TELEMAC-3D. This solver can provide velocity, salinity, temperature, and particle mass concentration fields derived from a set of partial differential equations describing their behaviour through space and time, based on the basic conservation laws of mechanics applied to fluid and particles. The equations, numerically discretized, are solved in a limited number of points (nodes) spread over the user-defined domain of interest. Neighbouring nodes are connected with straight lines, eventually generating a triangulated mesh: the computational grid. Derivatives in the equation are solved by assuming linear interpolation between values in the nodes.

After calibration and validation, the 3D numerical model shall be used to simulate scenarios of the North Sea plastic litter fates for a various range of periods, within an affordable computation time (CPU).

Resolved versus subgrid scale processes

The size of the computation grid strongly influences the computation's CPU time. The latter can be particularly restrictive for the contemplated simulations. However, the grid resolution determines the model quality: are the nodes numerous and close enough to capture the major gradients and variation rates of the fields of interest? The main answers rely on the physics of interest (section 2). In that sense, simulations of the 3D dynamics of microplastic particles, coupled with flow motion in the whole North Sea, may represent important challenges in terms of numerical resources and CPU time consumption.

But the most limiting factor is computation time: one wants the answer from the model within an acceptable time period (usually not more than one day, exceptionally a few days). The modelling of the motion of microplastic particles in the North Sea then faces enormous challenges in terms of scale problems.

To resolve the motion of an individual particle, one needs to work with computational meshes with distances smaller then at least one tenth of the particle size, in order to resolve the water motion around this particle and calculate the exchange of momentum (to determine the interacting forces). To resolve the water motion in the North Sea in 3D over a period of say one year within an acceptable time, one should limit the number of computational nodes maximally to the order of 1 million (Eskens, 2021). One can easily understand that both these conditions are not compatible.

Then, specific attention is paid for providing results from 3D computations that are physically meaningful and numerically reliable according to standard practice of the CFD science, and simultaneously, that are affordable in terms of CPU time consumptions. Therefore, one makes compromises. A multi-scale modelling approach needs to be considered to represent flow

properties or phenomena occurring at spatial scales smaller than the grid size (i.e. the internodal distance) of the computational grid. Such a (so-called) subgrid-scale modelling approach is applied to, for instance, turbulence modelling and wave modelling, or for bottom roughness and particles property closure formulations.

Coupled Eulerian-Lagrangian description

Most models applied to plastic litter motion in rivers or oceans use a Lagrangian particle-tracking approach. This approach assumes that the particle velocity equals the one of the surrounding water. Also, the tracer dynamics is considered having no impact on the water dynamics (i.e., the "passive-tracer" assumption). Such methodology can be simple and fast to operate since velocity fields of rivers and ocean are available online from various open-data oceanographic models. The user does not even need to understand how these data are generated. The method has been specifically popular for tracing floating plastic.

However, this method has several drawbacks. Computing the water dynamics independently from the dynamics of immersed particles may seriously affects the reliability of both resulting fields, especially in the case of fast evolving events (like storms). Besides, such approach only considers the drag contribution of the flow without inertial effects. Some models add a random walk component to consider the drift contribution generated by turbulence. Besides, few models add the drag contribution generated by waves. And Lagrangian models accounting for 3D effects, in particular the gravity field and the settling/rise behaviour, are not common.

The LABPLAS WP7 North Sea model aims to better understand the pathways of plastics in all 3D directions.

Such model is built with the TELEMAC-3D numerical solver, which allows to observe interactions between currents, waves, temperature, salinity, sediment and plastic concentrations, considering also external conditions, such as wind, atmospheric temperature, and astral potential. Do to so, TELEMAC-3D uses a coupled Eulerian-Lagrangian approach. Such a fundamental physics-based approach provides the most reliable solutions to simulate plastic litter dispersal in seas or oceans.

Note that TELEMAC also allows a coupled Eulerian-Lagrangian approach which combines the particle-tracking ability of the Lagrangian description with the continuum fluid momentum balance of the Eulerian description. As it keeps the disadvantages of particle-tracking, not allowing all physics to be represented accurately enough, this method is not withheld.

2 PHYSICS OF INTEREST

2.1 Hydrodynamics

The motion of water is the main driver of plastic litter transport and dispersal in the aquatic environment. We distinguish between the global motion, driven by pressure gradients, i.e. the *currents*, and the free surface motion by *waves*.

Currents

Pressure gradient driven water motion is characterized by the flow velocity (magnitude and direction, expressed as the 3D components of the velocity vector) and the pressure. Mathematically, these four parameters are obtained by the numerical solution of the fundamental equations of conservation of water mass and momentum.
An additional parameter is the water level, the elevation of the interface between water and air. The free surface changes continuously due to the different forces of the tide, wind swell, currents, earth rotation (Coriolis) and gravity. It can be computed as the solution of the kinematic equation of the free surface.
However, we will follow a simplification by assuming a hydrostatic pressure distribution, which removes the need to solve the kinematic condition, and the set of basic equations (mass balance + Reynolds-averaged Navier-Stokes equations + kinematic condition) is replaced by the shallow-water (or Saint-Venant) equations (see section 2.1).

Waves

Waves are a special free surface motion. The most important surface waves are those generated by the shearing force of the wind. Wave fields can be decomposed into sinusoidal motions of different amplitudes and wave lengths. The net motion under sinusoidal up-and-down motion is zero. But the wind causes the waves to propagate, and the net motion of water is no longer zero, but moves in the direction of the wind with a motion called the *Stokes drift*.

Since wind direction is generally uncoupled from tidal and currents, the *Stokes drift* may push floating plastic into a direction which deviates from the main current. This mechanism is known to be a major driver for beaching of plastic litter. In rivers, this happens due to waves generated by boats when displacing water during their motion.

The spatial dimensions and structure of waves are too complex to resolve explicitly and accurately on the large domain of the North Sea. Since the wave lengths of wind generated surface waves is smaller than the grid size, individual waves cannot be resolved. Instead the evolution of the total energy present in the waves is computed with an energy balance equation.

The energy per unit area is expressed as:

$$E = \sum_{m=1}^{M} \frac{1}{2} \rho g {a_m}^2 = \frac{1}{8} \rho g {H_S}^2 \qquad (2.1.)$$

where: a is the wave amplitude for each monochromatic wave in which the wave field can be decomposed, and H_S the significant wave height.

Since sea surface waves are the result of multiple wave interactions, the wave field is typically represented by a wave spectrum, obtain by applying a Fourrier transform on the measured variation of the sea surface elevation at a given location (typically from a wave buoy). The corresponding distribution in the frequency domain is often characterized by a JONSWAP spectrum, based on the field campaign, documented by Hasselmann *et al.* (1973):

$$E(f) = \alpha_{Ph} \frac{g^2}{(2\pi)^4 f^5} \exp\left[-\frac{5}{4}\left(\frac{f_p}{f}\right)^4\right] \gamma^{\exp\left[-\frac{1}{2\sigma^2}\left(\frac{f}{f_p}-1\right)^2\right]} \qquad (2.2.)$$

where: f is the frequency; $f_p = 22\left(\frac{g^2}{U_{10}F}\right)^{1/3}$; $\alpha_{Ph} = 0.076\left(\frac{{U_{10}}^2}{Fg}\right)^{0.22}$ is the Phillips constant; F is the fetch; $\gamma = 3.3$; $\sigma = \sigma_a = 0.07$ for $f < f_p$ and $\sigma = \sigma_b = 0.09$ for $f > f_p$. All parameter values are based on the JONSWAP experiment data.

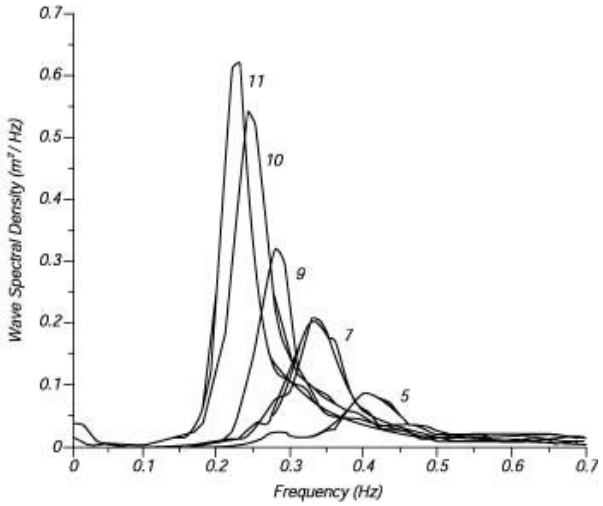

Figure 2.1 Wave spectra of a developing sea for different fetches according to Hasselmann et al. (1973).

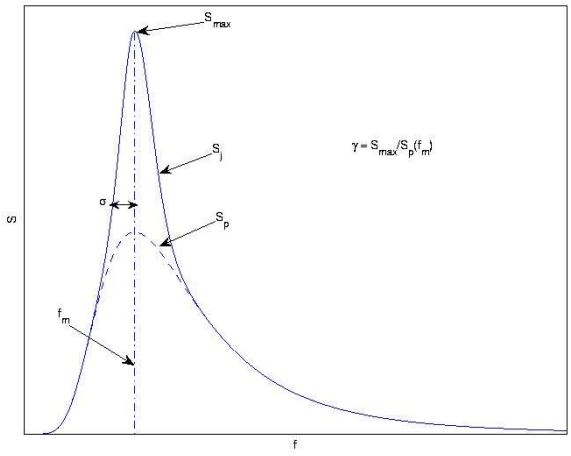

Figure 2.2 Comparison of the JONSWAP and Pierson-Moskowitz spectra (Source: WikiWaves.org)

The JONSWAP spectrum actually is a Pierson-Moskowitz spectrum multiplied by an extra peak enhancement factor (the last factor γ^r in eq.2.2); see Figure 2.2. This allows the waves to grow over distance, in accordance to reality.
For more background, see https://wikiwaves.org/Ocean-Wave_Spectra

Turbulence

Turbulence is the apparent chaotic behaviour of water when it flows. It is caused by instabilities at molecular scale, causing water molecules to be exchanged between neighbouring streamlines. It is the most difficult phenomenon of water motion to be described when studying water bodies larger than 1 litre. Turbulence can be simulated with high-resolution Navier-Stokes solvers (called "Direct Numerical Simulation"), but this method requires an extremely high grid resolution and small-time steps, which makes the computation immediately very costly and even impossible for a domain of the size of the North Sea.

At the scale of interest, turbulence is modelled through homogenization by diffusion and dispersal contributions within the averaged momentum equation. Following the Bakhmetiev analogy and Prandtl's mixing-length theory, turbulent momentum exchange has a net effect on the flow that is similar to the viscous shear stress effect. Therefore, as proposed by Boussinesq, the turbulent momentum flux (i.e. the divergence of the Reynolds stress) may be considered as a diffusive contribution, for which the related coefficient may be called the *eddy viscosity*. Similar considerations exist for particle dispersal.

This eddy viscosity is not a material property but depends on the strength of the flow field. Different semi-empirical turbulence closures have been proposed throughout the past decades. We chose one of the oldest that remains popular in coastal engineering (i.e. the k-epsilon model, designed for wall-generated turbulence), but only for the vertical turbulence which is governed by shear with the bottom.

The horizontal turbulence is described either as a constant value of the eddy viscosity or expressed with a Smagorinski model, a primitive version of LES (Large Eddy Simulation). The motivation to use another turbulence model in the horizontal is two-fold: 1) the horizontal grid spacing is 1-1000 times the vertical spacing, and therefore cannot capture all turbulent motion and vortices, and 2) the horizontal turbulence is not governed by shear with the shores, but rather by shear within the larger horizontal streams.

Bottom friction

In a 3D model with the k-epsilon turbulence model, the bottom friction is typically dealt with through a Nikuradse equivalent roughness closure to compute the bed shear stress from the computed vertical velocity profiles. The physical inner-boundary layer of the bottom layer is "skipped", i.e. not resolved, using a so-called wall-layer approach (which is based on the analytical Prandtl mixing-length turbulence closure) because its thickness is of subgrid scale relative to the vertical mesh layer thickness at the bottom. Values of equivalent roughness heights are determined based on the available information on sediment composition (section 5.8) and fine-tuned during the calibration step.

2.2 Temperature & Salinity

Unlike sediments, plastics are particles of quite light density. The range of plastic densities is close to water density and vary from 800 g/l to 1600 g/l ; while sediments density is more about 2650 g/l. Therefore, it is essential that the water density is computed the most precisely as possible to account for the correct deposition fluxes of plastics due to the water density effects.

The density of seawater is primarily influenced by the salinity (S), the temperature (T), and the pressure (p).

The water density formulation of Fonofoff & Millard (1983) will be used as a first approach. This expression depends only on temperature and salinity and is valid for temperature verifying 0 < T < 40 °C , for salinity verifying 0 ≤ S < 42 PSU and for pressures lower than 10 bar[1]. Density of pure water is first calculated as a function of the temperature alone. Based on this reference density value, the salinity and temperature dependent density value of water is calculated. The density-salinity-temperature relationship calculated using the below expressions is shown in the Figure 2.3.

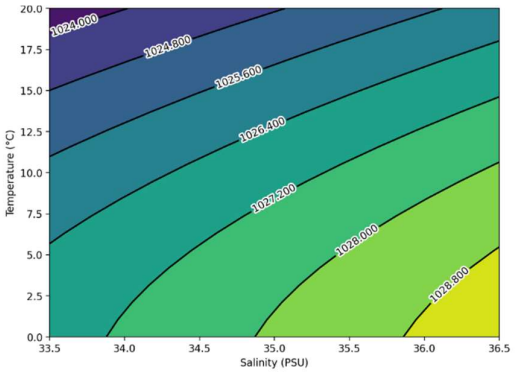

Figure 2.3 Salinity and temperature distribution depending on water density and calculated using the Fonofoff & Millard formulation (1983)

$$\rho_{purewater} = a_0 + a_1 T + a_2 T^2 + a_3 T^3 + a_4 T^4 + a_5 T^5 \quad (2.3.)$$

$$\rho(T,S) = \rho_{purewater} + (b_0 + b_1 T + b_2 T^2 + b_3 T^3 + b_4 T^4)S + (c_0 + c_1 T + c_2 T^2)S^{3/2} + d_0 S^2 \quad (2.4.)$$

where:

$a_0 = 999.84$	$a_1 = 6.8 \times 10^{-2}$	$a_2 = -9.1 \times 10^{-3}$	$a_3 = 10^{-4}$	$a_4 = -1.1 \times 10^{-6}$
$a_5 = 6.5 \times 10^{-9}$	$b_0 = 0.8245$	$b_1 = -4.1 \times 10^{-3}$	$b_2 = 7.64 \times 10^{-5}$	$b_3 = -8.25 \times 10^{-7}$
$b_4 = 5.4 \times 10^{-9}$	$c_0 = -5.7 \times 10^{-3}$	$c_1 = 10^{-4}$	$c_2 = -1.65 \times 10^{-6}$	$d_0 = 4.8 \times 10^{-4}$

To achieve the variable water density calculation in the numerical model, it is required to have the temperature and salinity values at all nodes of the domain. Since the domain of the model is small in geographical scale, temperature and salinity quantities are considered as passive tracers, provided that initial condition and boundary conditions are imposed. It is required to have correct initial condition in order to avoid longer warm-up period : 35 PSU and 16°C seem reasonable initial conditions of the North Sea region for computations starting in summer season (cf. paragraph 5.5).

[1] https://www.coastalwiki.org/wiki/Seawater_density#cite_note-1

The above water density formulation is quite appropriate for water depths in coastal areas and will be seriously questioned for the North Sea applications, since the pressure contribution might be much more significant far from coasts.

2.3 Particle transport and dispersal

Particles in a suspending medium (here water) are moved by the forces they undergo. Particles in water are subject to the forces of:

- drag by the water motion causing displacement in the direction of the flow, i.e. transport;
- gravity causing sedimentation (sinking) when the particle density is larger than that of the surrounding water (so-called buoyant particles), or rising when the particle density is smaller (so-called negative-buoyant particles);
- shear caused by velocity gradients in the flow field, which in its turn can cause particle rotation;
- turbulent drift caused by the chaotically directed turbulent drag on the particle. Turbulent drag is a major cause of dispersal, which can be represented by a diffusive process, as it results in reducing concentration gradients and equalizing concentrations.

Turbulent drift in water flowing over a (sediment) bottom counteracts gravity, resulting in an vertical particle concentration profile that is non-uniform, with the highest concentrations near the bottom for heavy particles (as upward turbulent drift keeps particles in suspension), and near the surface for floating particles (as these can be dragged down by this turbulent drift).

Plastic particles, with their low density, are much more susceptible to drag than the usually heavier sediment particles; even more when they are flexible and their shape is flat (i.e., foils) or needle-like (i.e., fibres).

The transport of particles goes at the cost of energy, which is extracted from the kinetic energy of the water motion and the potential energy from the water elevation. The total amount of particles that can be transported by the flow is thus limited to a level called the suspension capacity. In most referenced studies, plastic particles in sediments are underrepresented by several orders of magnitude relatively to minerals and organic particles naturally present is the medium. Therefore, transport of plastic particles among sediments must be more accurately considered in future models.

The transport of particles is governed by the particle mass balance (or particle transport) equation (section 3.5), where the settling velocity of the particle is the dominant particle property, necessary to solve the problem.

Settling velocity of particles

The concept of particle settling velocity has been used to model the plastic litter transport within earlier 2D computations verifying the shallow water assumption. Related formulations are reminded thereafter.

Following the conclusions from the Deliverable 7.8 (Pedrotti *et al.*, 2003), the settling velocity is computed with the Turton-Clarke (1987) formula, consisting of a power blending of the asymptotic behaviour from the Stokes solution to a constant value at very high Reynolds numbers:

$$w_* = \left(\left(\frac{{d_*}^2}{A} \right)^{-n} + \left(\frac{\sqrt{d_*}}{B} \right)^{-n} \right)^{-1/n} \tag{2.5.}$$

with A, B and n empirical parameters, and where the settling velocity (w_p) is non-dimensionalized as:

$$w_* = \frac{w_p}{(g'\upsilon)^{1/3}} \tag{2.6.}$$

where: $g' = (\gamma - 1)g$ is the buoyancy corrected gravity and $\gamma = \rho_p/\rho_f$ = is the specific particle density.

The same scales are used to define an alternative Reynolds number:

$$d_* = d\frac{(g'\nu)^{1/3}}{\upsilon} = d\left(\frac{g'}{\upsilon^2}\right)^{1/3} \tag{2.7.}$$

d is the particle diameter and d_* is the non-dimensional diameter that equals the third root of the Archimedes number (Ar), the ratio of buoyancy force to the viscous force (formulation available on the web page https://en.wikipedia.org/wiki/Archimedes_number).

The parameter values ($n = 1$, $A = 24$ and $B = 1$) for particles with a Corey shape factor of $\psi_C = 0.7$ are recommended (similar as for natural sand, Cheng, 1997) to be applied for plastic particles with shape factors between 1 and 0.4, since the data collection by Kramer *et al.* (2021) demonstrates that the uncertainty on the drag determination is large (i.e. $\psi_C = 0.7 \pm 0.3$).

For particles with smaller shape factors ($\psi_C < 0.4$), typically flat “disks” (i.e. foils) and long “needles” (i.e. fibres, $\psi_C < 0.1$), the definition of a stable settling velocity is problematic. Moreover, foils and fibers are very deformable, and open-folded foils are easily dragged along by currents (acting like a parachute). Therefore, these particles are not explicitly considered in the present study.

Floating plastic transport

Since the vertical layers in the model need to be coarse for generating results at an acceptable computational coast (section 2), the accumulation at the water surface of negatively buoyant plastics requires a separate approach. This can be modelled with the new module for floating plastics proposed by Riom *et al*. (2022). It actually mimics the methodology applied to bedload transport for buoyant particles (sediments and heavy plastics), but projected to the surface. It solves the mass balance at the water surface taking into account advection by currents, turbulent drift, wave drift and wind forcing.

Size distribution effects

The large range of size of plastic litter particles and its variation can be captured mathematically by the application of the Population Balance Equations (PBE) and the Quadrature of Method of Moments (QMOM). This methodology has been implemented into TELEMAC by Shettigar *et al.* (2024), and allows to study the evolution of the mean size and its standard deviation of the assumed log-normal distributed particle size in every node of the computational domain.

Aggregation

The smaller plastic particles become, especially when < 10µm, the more likely surface charges that are no longer cancelled out will be generated allowing the particles to become hydrophobic or hydrophilic and aggregate with each other (= homo-aggregation). This aggregation effect between plastic particles is not considered because its likeliness is small considering the low concentrations found in field samples.

However, hetero-aggregation with the much more abundant mineral and organic particles is very likely. Therefore, it is assumed that plastic particles are caught in cohesive sediment flocs, which are typically found in turbid regions in estuaries, i.e. turbidity maxima. The particle will then be settling with the fall velocity of the floc.

In order to take this process into account, it is necessary to also compute sediment transport, to determine the suspended particle matter (SPM) concentrations. There is significant knowledge about aggregation and break-up of cohesive sediment flocs.

Fragmentation

Because fragmentation can start at different moments for each of the particles and at different rates depending on the polymer and the fragmentation mechanism, this effect is not explicitly accounted for. It is somewhat compensated by applying a size distribution to the particles, since the net effect would disappear in the noise on the particle property data. Moreover, the model runs simulate periods much shorter than the known slow fragmentation rates.

Biofouling

The effect of biofouling is not explicitly accounted for because its change disappears in the noise of the uncertainty of determining the fall velocity. Moreover, it is impossible to know the age of particles and the moment that biofouling starts for each individual particle. Therefore, it is assumed that biofouling implicitly is accounted for in the settling velocity distribution.

3 THE TELEMAC-3D SOLVER

TELEMAC-3D is an open-source hydrodynamic solver that is based on the finite element method and available for download on the web page www.openTELEMAC.org. The main equations involved in the 3D North Sea model, built-up to simulate plastic litter transport, are described thereafter.

3.1 Hydrodynamics

TELEMAC-3D module solves the advection-diffusion equation for the flow velocity, the water depth and tracer concentrations. TELEMAC-3D finds wide applications, such as hydrodynamics of coasts, deep sea, estuaries, rivers or lakes. Processes like tidal currents and thermohaline circulation and/or stratification can be simulated, considering physical contributions such as Coriolis force, bottom friction, rainfall, or heat exchanges at the water-atmosphere interface.

The TELEMAC-3D solver provides fluid dynamics solutions according to the following assumptions:

- 3D equations with a time variable free surface,
- Incompressible fluid - No considerable density variations in the mass conservation equation,
- Hydrostatic pressure hypothesis – Pressure at a given depth is the sum of the air pressure at the fluid surface plus the weight of the overlaying water mass,
- Boussinesq approximation of the momentum; the density variations are only taken into account as buoyant forces.

With the above assumptions, the 3D equations that are solved are:

Mass conservation equation:

$$\frac{\partial U}{\partial x}+\frac{\partial V}{\partial y}+\frac{\partial W}{\partial z}=0 \tag{3.1}$$

Momentum conservation equations in x and y direction:

$$\frac{\partial U}{\partial t}+U\frac{\partial U}{\partial x}+V\frac{\partial U}{\partial y}+W\frac{\partial U}{\partial z}=-g\frac{\partial Z_s}{\partial x}+\frac{1}{h}\mathrm{div}(h\upsilon_e\mathrm{grad}(U))+F_x \tag{3.2}$$

$$\frac{\partial V}{\partial t}+U\frac{\partial V}{\partial x}+V\frac{\partial V}{\partial y}+W\frac{\partial V}{\partial z}=-g\frac{\partial Z_s}{\partial y}+\frac{1}{h}\mathrm{div}(h\upsilon_e\mathrm{grad}(V))+F_y \tag{3.3}$$

Pressure equation (replacing the full z momentum):

$$p=p_{atm}+\rho_o g(Z_s-z)+\rho_o g\int_z^{Z_s}\frac{\Delta\rho}{\rho_o}dz' \tag{3.4}$$

where: t is the time, (x, y, z) are the three Cartesian coordinates, (U, V, W) are the velocity components in the three Cartesian coordinate directions, Z_s is the free surface elevation, h is the water depth, p is the pressure, p_{atm} is the atmospheric pressure, g is the acceleration due to gravity, v_e is the effective kinematic viscosity (the sum of molecular and turbulent eddy viscosity) of the flow, ρ_o is the reference water density and F_x and F_y are the momentum source terms such as wind, Coriolis force or bottom friction.

3.2 Waves[2]

The TOMAWAC module is used to model the distribution and propagation of wave energy inside the domain (Benoit *et al.*, 1996). To this end it solves the wave action balance equation:

$$\frac{\partial N}{\partial t} + \dot{x}\frac{\partial N}{\partial x} + \dot{y}\frac{\partial N}{\partial y} + \dot{k}_x\frac{\partial N}{\partial k_x} + \dot{k}_y\frac{\partial N}{\partial k_y} = Q(x, y, k_x, k_y, t) \tag{3.5}$$

where N is the wave action density, defined as:

$$N(x, y, k_x, k_y, t) = \frac{F(x, y, k_x, k_y, t)N}{\sigma} \tag{3.6}$$

$F(x, y, k_x, k_y)$ is the wave energy spectrum, $\boldsymbol{k} = (k_x, k_y)$ is the wave number vector, σ = the intrinsic frequency. σ and k $(= ||\boldsymbol{k}||)$ are related through the dispersion relationship:

$$\sigma^2 = gk\tanh(kh) \tag{3.7}$$

with h the water depth.

In the case of a current $\boldsymbol{U} = (u_x, u_y)$, the intrinsic (or relative) frequency is the frequency in the moving frame of reference (frame moving with the current). The relation between the absolute frequency ω and σ is given by:

$$\omega = \sigma + \boldsymbol{k} \cdot \boldsymbol{U} \tag{3.8}$$

$Q\ (x, y, k_x, k_y, t)$ represents the source terms: energy input by wind, redistribution of energy over the spectrum trough non-linear wave-wave interactions (quadruplets: 4 wave interaction, triads: three-wave interactions) and dissipation of energy through white-capping, bottom friction dissipation, depth induced breaking, dissipation due to vegetation, …

The $\dot{x}$, $\dot{y}$, $\dot{k}_x$ and $\dot{k}_y$ refer to propagation velocity in geographical space and wavenumber space respectively. That waves can propagate from one location to another (geographical space) is easy to comprehend. Wave propagation in spectral space is typically seen as a change of wave direction (think of refraction through changing water depth or current field) or change in absolute frequency

[2] Reviewed and complemented by Prof. Jaak Monbaliu, KU Leuven's ocean waves expert.

(think of Doppler shift). For full details the reader is referred to a standard reference book, such as Holthuijsen (2007).

Further details on the implementation in the TELEAMC suite can be found in the Tomawac User's Manual, downloadable from www.openTELEMAC.org.

To solve the wave action balance equation, a spectral discretization needs to be chosen. Typically this is done in frequency-direction space (directly related to wavenumber space through the dispersion relationship). A frequency discretization over 25 frequencies and 12 or 24 direction is common practice for shelf sea applications. The first frequency is typically chosen around 0.04 Hz with a logarithmic scaling for the other frequencies, i.e. $\sigma_{i+1}=1.1\ \sigma_i$). To run the model, wind input is needed from e.g. meteorological datasets such as the ECMWF Reanalysis v5 (ERA5) (*see link in references*). Time steps in the model need to be chosen according to the properties of the calculation mesh.

Unless all waves of interest can be generated inside the model domain, boundary conditions in the form of a wave spectra need to be provided. They can be provided by running first a larger scale TOMAWAC model or they can be extracted from archived wave spectra such as the ECMWF Reanalysis v5 (ERA5) dataset[3].

The nested wave model is forced at the open boundaries with spectral wave energy from the North Sea model.

As can be seen in the equations, waves are affected by currents (and water depth) and vice-versa currents are also affected by waves. To this end the wave model and hydrodynamics need to exchange information in order to use up to date information. The coupling between Telemac and Tomawac is achieved through a coupling module. In order to reduce the computational cost of the wave module, the resolution of the TOMAWAC wave model computation grid can be different from the resolution of the TELEMAC hydrodynamic model grid. The exchange of variables between Telemac and Tomawac is achieved with spatial interpolation of the parameters over the three closest nodes of the other mesh using weights based on inverse distance. The impact of Interpolation approximations can be reduced by developing the meshes jointly, so that the coarser mesh points (i.e. the Tomawac nodes) coincide with the finer mesh points. Details on the used coupling module TEL2TOM can be found in (Breugem *et al.*, 2019).

3.3 Active tracers

Tracers can be any quantities which are transported in the water. For example, temperature, salinity, sediments, etc. When the tracer affects hydrodynamics, by their inertia or by changing water

[3] https://www.ecmwf.int/en/forecasts/dataset/ecmwf-reanalysis-v5

density or viscosity for instance, they are considered as *active tracers*. Otherwise, they are considered as *passive tracers*. The common active tracers are fluid temperature and salinity which affect both the flow density and viscosity. Particles can also be considered as an active tracer when it affects the flow velocities and turbulent dissipation. The processes affecting the evolution of tracers are the flow of the water (advection), (turbulent) diffusion and various source and/or sink terms. The 3D formulation of the tracer transport equation is:

$$\frac{\partial T}{\partial t} + U\frac{\partial T}{\partial x} + V\frac{\partial T}{\partial y} + W\frac{\partial T}{\partial z} = \frac{\partial}{\partial x}\left(\upsilon_T \frac{\partial T}{\partial x}\right) + \frac{\partial}{\partial y}\left(\upsilon_T \frac{\partial T}{\partial y}\right) + \frac{\partial}{\partial z}\left(\upsilon_T \frac{\partial T}{\partial z}\right) + Q \qquad (3.9)$$

T is the tracer quantity of interest, Q is the source or sink term and υ_T is the tracer diffusion coefficient, in turbulent flow usually assumed to be proportional to the eddy viscosity.

Salinity

Salinity is modelled as an active tracer, affecting the water density, with no source or sink terms. Its dispersal is governed by advection-diffusion and the prescribed boundary conditions. It requires data as boundary conditions at the open sea boundary and the at the river inlets. Salinity evolution due to rainfall is considered to be negligible. The effects of rainfall are indirectly taken into account by prescribing river boundaries whose discharge values are in relation to the precipitations. Therefore, no surface or bottom boundary condition are necessary for salinity modelling

Temperature

Temperature is modelled as an active tracer, affecting the water density. Its dispersal is governed by advection, diffusion and the prescribed boundary conditions including the surface and bottom boundary condition. The temperature field is strongly influenced by radiation exchange with the atmosphere. The air temperature and wind velocity which are the driving forces of the temperature evolution in water columns are derived from meteorological models. For the sea bottom, a constant temperature is assumed.

3.4 Heat exchanges with the atmosphere

The temperature boundary condition at the water-atmosphere interface involve the contribution of the atmospheric radiation *RA*, of the water radiation *RE*, of the latent heat due to evaporation *CE* and the sensitive heat of convective nature *CV*. The complete balance of exchanged fluxes at the water-atmosphere interface is written:

$$\left(K\frac{\partial T}{\partial z}\right)_{z=\eta} = \frac{RA - RE - CE - CV}{\rho\, C_p} \qquad (3.10)$$

where: K is the coefficient of molecular heat diffusion in water, ρ is the water density and C_p = 4180 J/kg/°C.

The penetration of the solar radiation in the water column involves the solar radiation flux *RS* and contribute to the flow heat balance as a source term S of the advection-diffusion equation of the temperature:

$$S = \frac{1}{\rho\, C_p} \frac{\partial Q(z, RS)}{\partial z} \tag{3.11}$$

$Q(z, RS)$ is the residual solar radiation at the elevation z.
Formulations of *RA*, *RE*, *CE*, *CV* and *RS* are specified in the TELEMAC-3D Theory guide. And we paid attention that estimations of theses fluxes required specific meteorological data: the wind magnitude and direction, the air temperature, the atmospheric pressure, the relative humidity, the nebulosity, and the rainfall.

3.5 Particle transport

Unlike the majority of plastic dispersal models, based on passive tracer assumptions and Lagrangean particle tracking, the present modelling approach considers a coupled Eulerian-Eulerian modelling of particle concentrations. This requires the solution of the particle mass balance equation, including advection and diffusion. Whereas advection described the transport by fluid drag on the particles, diffusion describes the net drift by turbulence. The following formulations are written according to a strictly Eulerian description.

GAIA is the sediment transport module of the TELEMAC modelling suite (Tassi *et al.*, 2023). The suspended sediment transport is still handled by the advection-diffusion equation applied to the sediment concentration in TELEMAC-3D. GAIA handles the bed evolution, bed load transport and processes at the bottom such as erosion and deposition fluxes. It is therefore obvious that TELEMAC-3D is coupled to GAIA. It is also possible to have coupling of GAIA and TOMAWAC as well as with water quality model of TELEMAC. In the sections below, the individual processes that are of significance for sediment transport model are explained.

Suspension transport

In 3D cases, the suspended particle transport solved with the use of the advection-diffusion equation:

$$\frac{\partial C}{\partial t} + \frac{\partial UC}{\partial x} + \frac{\partial VC}{\partial y} + \frac{\partial}{\partial z}(W - w_p)C = \frac{\partial}{\partial x}\left(\varepsilon_p \frac{\partial C}{\partial x}\right) + \frac{\partial}{\partial y}\left(\varepsilon_p \frac{\partial C}{\partial y}\right) + \frac{\partial}{\partial z}\left(\varepsilon_p \frac{\partial C}{\partial z}\right) \tag{3.12}$$

where: $C = C(x, y, z, t)$ is the concentration of the suspended particle, w_p is the particle settling velocity and ε_p is the turbulent diffusivity, assumed to be proportional to the eddy viscosity.

The bottom boundary condition is given by the bottom flux in balance with the source terms representing the exchange with the bed (in the case of cohesive sediments in the absence of fluid mud) or the bed load layer (in the case of sand or fluid mud) in terms of deposition and erosion, and is expressed as follows:

$$\left(\varepsilon_p \frac{\partial C}{\partial z} + w_p C\right)_{z=Z_b} = D - E \tag{3.13}$$

where Z_b is the bed level, D is the deposition flux and E is the erosion flux.

The change of the bed level elevation as the net result of erosion and deposition in the case of bed load transport is expressed by the bed surface mass balance equation, known as the Exner equation:

$$(1-n)\frac{\partial Z_b}{\partial t} + \frac{\partial q_b}{\partial x} = E - D \tag{3.14}$$

with: n the bed porosity, and q_b the (volumetric) bed load transport flux, computed with one of the available empirical transport equations.

Deposition

The deposition of the microplastics is considered to be affected by the suspended sediments. The hydraulic condition when the microplastic deposit is considered to be the same as in case of the sediments. The condition at which sediments settle is determined using the suspension capacity theory to get a space-time varying critical deposition shear stress for the sediments. In the sections below it is discussed in detail.

A novel deposition criterion, derived from Toorman's (2000 & 2002) suspension capacity condition is utilised in this work. Unlike previous methods, this criterion enables the estimation of the critical stress for deposition at each node without the necessity for calibration. As shear flow induces turbulence, the critical shear stress for deposition is correlated with the overall turbulent energy needed to sustain suspended sediment particles. When the bed shear fails to supply sufficient turbulent energy to keep the suspended particles in the water column, deposition initiates. The surplus sediment settles until the energy balance is reinstated. To address sand-mud mixtures, the critical shear stress for deposition, derived through the inversion of Toorman's suspension capacity criterion, is divided into two components. In such scenarios, the total required turbulent energy is distributed between the sediment fractions - a portion is allocated to maintaining non-cohesive particles in suspension, while the remainder is dedicated to keeping cohesive particles suspended. Following this theory, the critical deposition shear stress is given by:

$$\tau_{cd,m} = \frac{(1-\rho_w/\rho_m)\, g h}{R f_m} \frac{w_m\, C_m}{U} \tag{3.15}$$

where Rf_m is the limiting flux Richardson number of mud, closed with the following empirical relationship:

$$Rf_m = 0.25\left(\frac{u_*}{w_m}\right)^2 \frac{0.01}{1 + 0.01\left(\frac{u_*}{w_m}\right)^2} \tag{3.16}$$

u_* is the bed shear velocity, w_m is the settling velocity of the mud, C_m is the mud concentration in suspension, U is the magnitude of the velocity, g is the acceleration due to gravity and h is the flow depth. The critical deposition shear stress determined from this expression is also used for the deposition flux calculation for the microplastics. The assumption is based on the hypothesis that the microplastics themselves does not affect the flow or the turbulence characteristics and that the microplastics deposition is not independent from the deposition of the cohesive sediments.
Finally, the deposition flux is expressed as:

$$D = w_p C_p \left(1 - \frac{\tau_b}{\tau_{cd,m}}\right) \tag{3.17}$$

where w_p is the plastic settling velocity, C_p is the plastic concentration in suspension and τ_b is the bed shear stress < $\tau_{cd,m}$.

Erosion

The erosion of the microplastics from the bottom is not well established from either the field studies or the laboratory studies. The bottom of the domain also consists of the cohesive and non-cohesive sediments which have impact on the erosion behaviour of the microplastics. The most basic assumption that can be made in the absence of any data is that microplastics are able to erode from the bottom at the same moment as the sediments. This simply means, that the critical erosion shear stress of the microplastic is considered to be same as for the sediment in the bottom. To achieve this, we use mixed-sediment erosion formulation of Waeles (2005) and implemented for the Scheldt Estuary and Belgian coast in the work of Bi (2015). According to the mixed-sediment erosion formulation, the sand-mud mixture behaviour can be categorised into three regimes - non-cohesive, mixed and cohesive - based on the sand-mud mass fractional values. In the case of Scheldt Estuary, the threshold mud fraction (f_m) is considered to be 30 % and 50 %. The mixed sediment erosion behaviour is considered to be the same as pure sand when the mud fraction is less than 30 %. Similarly, it is considered to be same as pure mud when the mud fraction is greater than 50 %. Between 30 % and 50 % of mud fractions, the mixed criteria is applied. The critical erosion shear stress is calculated as follows:

For **non-cohesive (sand) regime (f_m < 30 %)**, the value is equal to the critical shear stress of the non-cohesive sediment fraction, with a correction that increases the critical shear stress to account for the cohesive sediment fraction:

$$\tau_{ce} = \tau_{ce,s} + x_1 f_m \quad (3.18)$$

For **cohesive regime (f_m >50%)**, the value is equal to the critical shear stress of the cohesive sediment fraction:

$$\tau_{ce} = \tau_{ce,m} \quad (3.19)$$

For the **mixture regime (30 % < f_m < 50 %)**, the value is computed by linear interpolation of values computed from the two previous cases:

$$\tau_{ce} = \frac{\tau_{ce,s} + x_1 f_{m,crit}}{f_{m,crit^*} - f_{m,crit}} \left(f_{m,crit^*} - f_m\right) + \frac{f_m - f_{m,crit}}{f_{m,crit^*} - f_{m,crit}} \tau_{ce,m} \quad (3.20)$$

$\tau_{ce}, \tau_{ce,s}$ and $\tau_{ce,m}$ are the critical erosion shear stress of the mixture, sand and mud respectively; $x_1$is the calibration constant; $f_{m,crit}$ and $f_{m,crit^*}$ are the lower and upper critical mud fraction values respectively.

The erosion rate if the mass mud fraction of the mixture is:

- f_m < 30%, its value is equal to the erosion rate computed for the sand fraction
- f_m > 50%, its value is equal to the erosion rate for mud fraction
- 30 % < f_m < 50 %, its value is computed by linear interpolation of values computed from the two previous cases

Finally, the erosion flux is expressed as:

$$E = M \left(\frac{\tau_b}{\tau_{ce}} - 1\right) \quad (3.21)$$

M is the erosion rate constant and τ_{ce} is the critical erosion shear stress > τ_b .

4 COMPUTATION SET-UP

4.1 General considerations

The standard practice for building a computational grid consists in : 1) defining assumptions about the major spatial variation rates of the continuum, and 2) ensuring a number of elements that is appropriate and sufficient regarding the precision order of the numerical schemes involved in the solver.

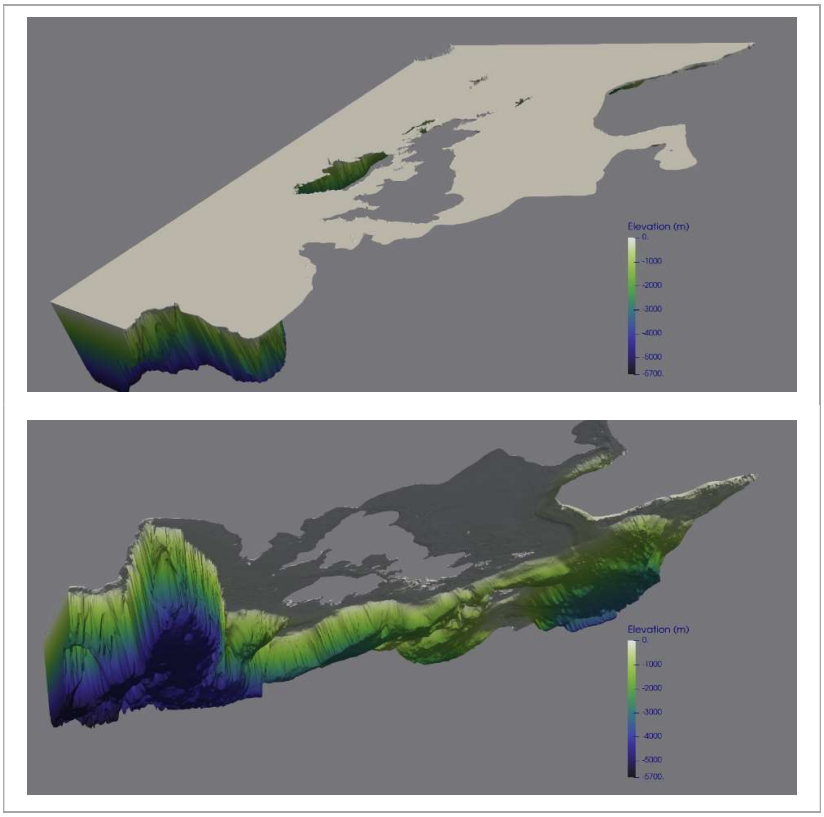

Figure 4.1 Bedrock 3D rendering of the fluid domain of interest comprising the northern European continental shelf with an averaged depth of 100 m order, and the closest Atlantic Ocean region showing a maximum depth of 6 km.

In the case of simple and smooth geometries, we commonly estimate the boundary layer thickness at walls vicinity to better stand for the regions along which the fluid particles, initially stuck to walls, progressively evolve from a presumed-quasi-static state to a dynamic-quasi-steady-well-ordered state: in other words, we estimate the layer thickness inside which shear and turbulent processes are dominant. After this estimation, an appropriate spatial discretization of boundary layers is applied to ensure an effective simulation of these layer detachments, and consequently, an effective simulation of the large-scale eddies in the flow.

In the case of the European North Sea, a classical boundary layer analysis is theoretical possible but not relevant in practice, because its geomorphology shows a bedrock that is particularly craggy, with plentiful and impressive singularities clearly visible at the modelling scale of interest. And these numerous morphologic singularities seem to be directly involved in the development of the most juvenile eddies that may support in return the development of the largest eddies in the flow. So then, the remaining criteria available to build the computational grid of the North Sea is finally the bedrock variability.

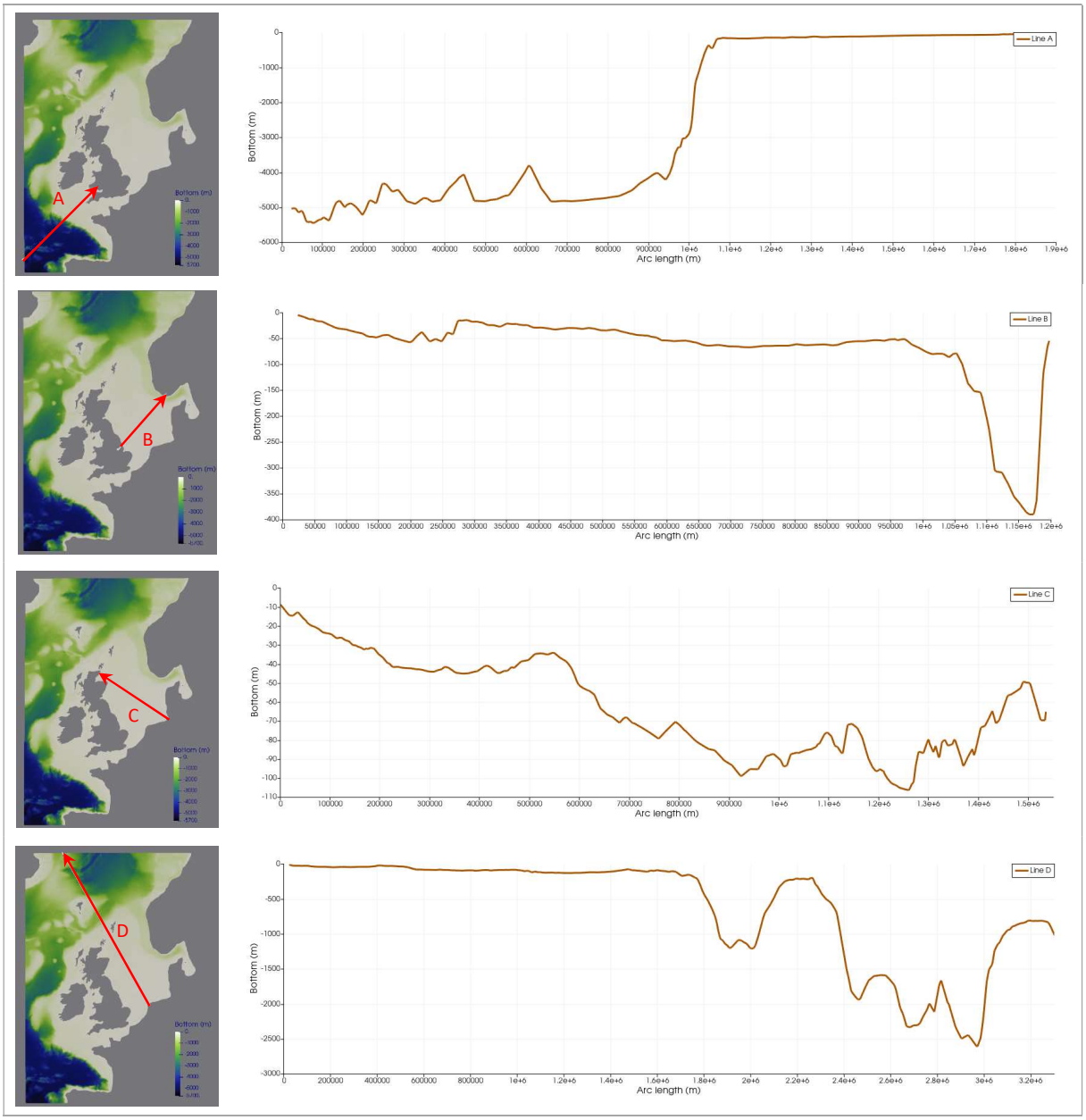

Figure 4.2 Bedrock variability of the fluid domain of interest according to plots over lines

The North Sea fluid domain is extremely thin, relative to its horizontal extend. Its global bedrock is of 100 m depth order whereas its characteristic length according to longitude or latitude is of 1000 km size order: the ratio between vertical and horizontal characteristic lengths is then of 10^{-4} order.

The latter observations about the thickness, the geomorphology and the high level of turbulence of the North Sea flow indicate that this region is probably dominated by convective contributions of tidal currents and atmospheric forces. However, the diffusive processes are expected to be more important in Atlantic areas, especially where the water depth can reach up to 6 km. So then, we need to estimate the respective contributions of momentum diffusion and convection first within the continental shelf region, and next within the Atlantic region surrounding the North Sea.

Understanding the real contribution of diffusion processes in the North Sea is even more important given that a high level of uncertainty exists concerning the diffusion coefficients that are appropriate to simulate momentum, temperature, and salinity transports in this flow region. To date, the available solution to obtain reliable diffusion coefficients is to compute them explicitly at the microscopic scale of specific control volumes.

Microscopic scale refers to the modelling scale of continuum and requires a computational grid made of elements the most fine as possible. Also, a *control volume* refers to the continuum system in which momentum, energy or any tracer balance is written to finally get the partial differential equations that mathematically model their dynamics in space and time. Whatever the method is based on (finite elements, finite volumes, or finite differences), each singular element of a computational grid always refers to an equivalent control volume of the continuum system, inside which momentum, energy or any tracer balance is written according to the type of material involved, and namely, according to its specific state or behaviour.

Concerning momentum, for instance, the "*type of material involved"* is modelled through the *Cauchy stress tensor* $\boldsymbol{\sigma}$, which law is often presumed to be linear with the *strain-rate tensor* $\boldsymbol{s}$; and simultaneously, this "*type of material involved"* is modelled through a certain value of the *dynamic molecular viscosity* μ that has been estimated itself within the latter presumption on Cauchy stress tensor linearity. Linearity between stress and strain tensors refers to the *Newtonian flow assumption*.

Regarding the high level of turbulence of the North Sea flow, we are aware that presumptions concerning the linearity of the Cauchy stress tensor may not be valid at the scale of interest, and that non-linear laws shall be seriously considered.

In the current study, we neglect the impact of immerged living systems on the global North Sea hydrodynamics. Then an important stage of the current study will be to verify through the momentum balance that shear stress quantities computed over a given control volume are well linear with the strain-rate quantities. Such inspection is important in order to : 1) ensure that the flow of interest does verify the *Newtonian flow assumption*, and consequently 2) ensure that we

are able to extract the diffusion coefficients values that are appropriate to the fluid system of interest.

Finally - and regarding the above considerations - the data of reference we foresee to use to validate our 3D hydrodynamic computations rely preferentially on in-situ measurements rather than on numerical models whose governing equations may be based on a Cauchy stress tensor law or diffusion coefficients that may not be appropriated for the specific fluid system of interest.

4.2 Numerical domain

The computational domain of interest comprises the North Sea and the entire continental shelf stretching from Norway to Galicia. This allows to dampen out numerical boundary effects and to consider weather conditions over a larger area, including offshore events such as storms or hurricanes.

Preliminary studies on North-Sea subdomains are currently in process to conclude on the appropriate minimum grid element size we must use to build the computational grid of the whole fluid domain. The appropriate minimum grid element size is determined according to the minimum control volume size for which the estimation of diffusion coefficient is stabilized under microscopic simulations.

Once the minimum grid element size is determined, it will be possible to build the final computational grid of the North Sea with elements bigger than the determined minimum size. In addition, the presumed final grid must be submitted to a convergence analysis to be considered as reliable.

To highlight the concept of computational grid, we describe hereafter a first prototype as an illustration. This prototype is based on a 2D grid made of elements with a default edge of 60 km length order: the total number of 2D nodes reach 60 517. Smaller edges are laid out over regions showing slopes that are particularly sharp. If we consider a spatial discretization of 16 levels along the water column, the total number of 3D nodes reach 968 272. Figure 4.4 and Figure 4.5 provide insights of such 2D and 3D distributions. The total number of elements mentioned above are rough estimations and the final computational grid may show a total number of elements slightly different regarding the results of the grid convergence analysis.

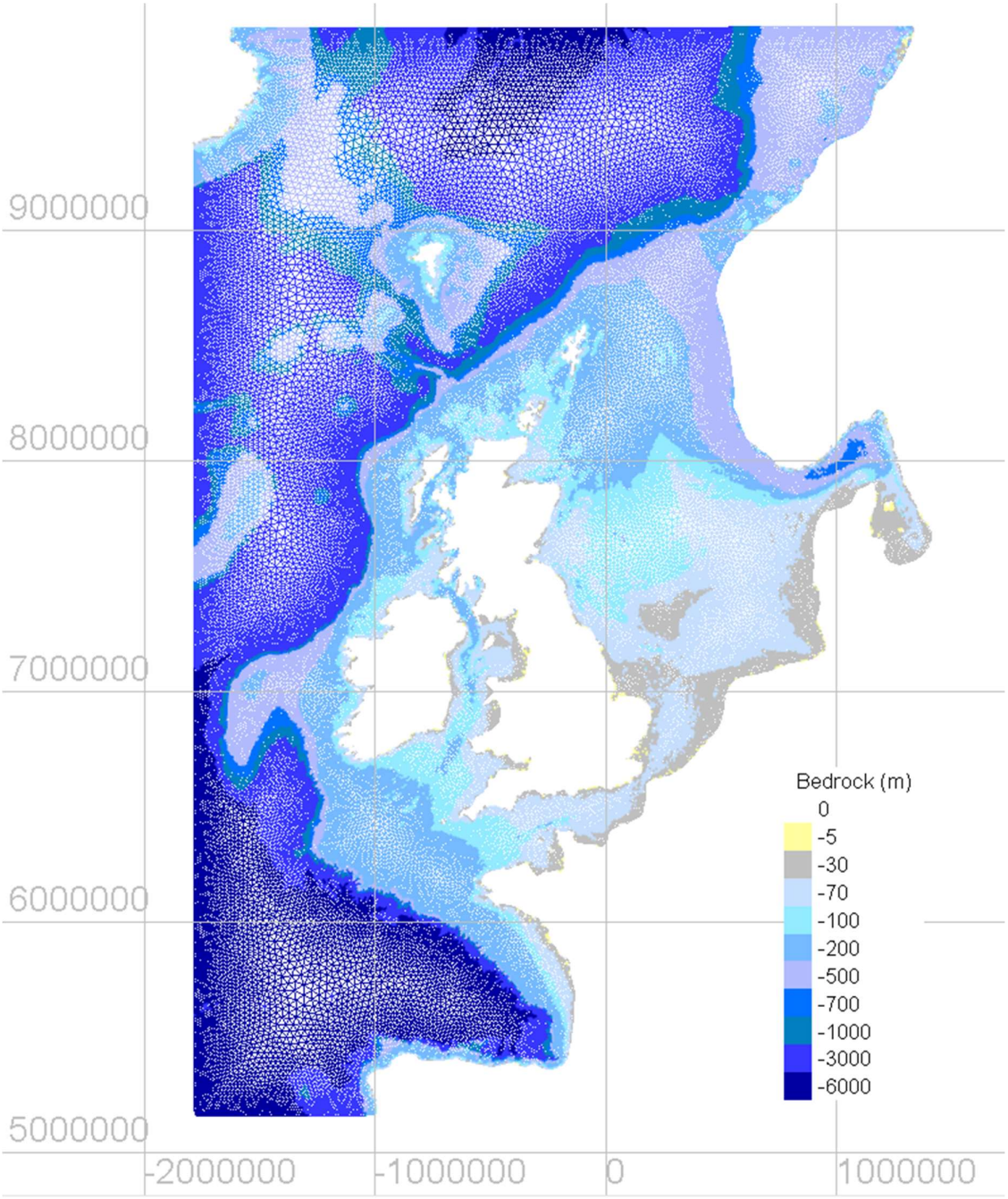

Figure 4.3 Bedrock data mapped on the 2D computational grid of the fluid domain of interest

Figure 4.4 Node layout of the 2D computational grid

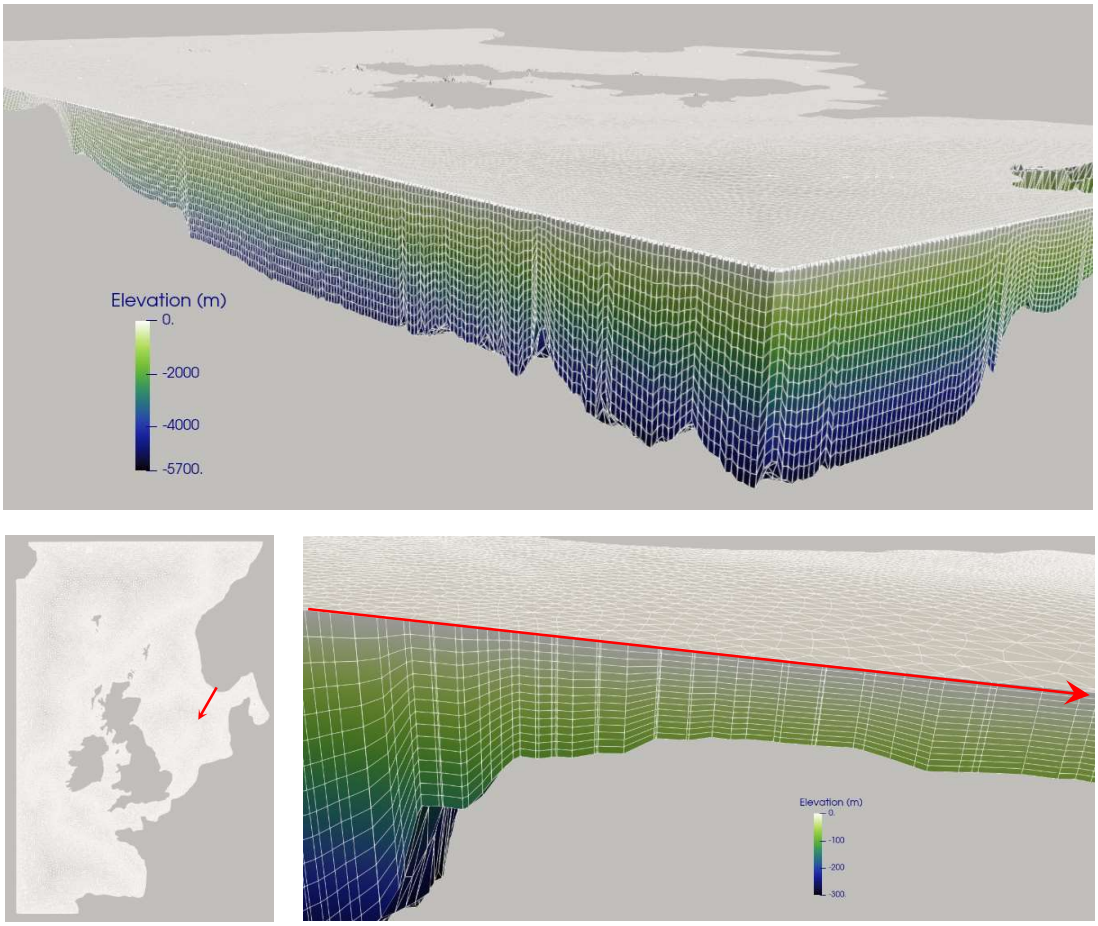

Figure 4.5 Water column node distribution of the 3D computational grid for 16 horizontal levels : the top view shows the node distribution along the south-west boundaries open on ocean and the bottom view shows the node distribution along a slice localised in the North Sea region, close to the Norway coasts.

4.3 Diffusion coefficients

Regarding the high level of stresses and turbulence exerted on the North Sea flow, it is obvious that the *dynamic molecular viscosity* μ quantified under laminar macroscopic states is not suitable to undertake the simulation of such fluid system. In Computational Fluid Dynamic, we often use the *momentum diffusion coefficient v* (also called the *kinematic viscosity*) that represents the ratio of the dynamic molecular viscosity μ over the *flow density ρ*. For freshwater flow under standard atmospheric condition at 20°C and laminar states, the dynamic viscosity verifies $\mu = 10^{-3}$ Pa.s and the kinematic viscosity (or momentum diffusion coefficient) $\nu = 10^{-6}$ m^2/s. These values are corrected to take into account salinity and temperature (section 2.2).

Several studies dealing with 3D simulations of the North Sea flow have been conducted with the help of momentum diffusion coefficients that are notably different in order to account for the much higher diffusivity of turbulent mixing. For instance :

- the 3D General Estuarine Transport Model (GETM) invested in Pätsch *et al.* (2017) use a lateral viscosity of 15 m^2/s in the central North Sea area, a value of 100 m^2/s in the vicinity of coastal regions and divided the latter values by 2 to define the related horizontal viscosities, since the Prandtl number had been assumed equalling 2 ;
- the 3D HAMburg Shelf-Ocean Model (HAMSOM), also investigated in Pätsch *et al.* (2017), indicates an averaged horizontal diffusion coefficient of 50 m^2/s order, with maximum values of 2000 m^2/s near the coast, and values in the central North Sea smaller than 20 m^2/s ;
- the Regional Ocean Modeling System Model (ROMS) invested in Ivanov *et al.* (2020) study use a horizontal diffusion coefficient of 25 m^2/s on coarse-resolution gridded regions and 1 m^2/s on high-resolution gridded regions ;
- the Regional Ocean Modeling System (ROMS) investigated in Klonaris *et al.* (2021) indicates a maximum value of 5.0 m^2/s for the horizontal diffusion coefficient.

For the same fluid dynamic system, these latter studies use momentum diffusion coefficients that are notably different from each other, which is quite understandable because this parameter depends on the modelling process itself, namely : 1) the control volume size within which the global momentum balance is observed, and 2) the macroscopic state of the flow within the selected control volume.

In practice, the optimal value to be used is determined by the model structure and grid sizes, and is usually determined by trial-and-error to generate numerically stable results. The coarse mesh does not allow a suitable modelling of the vortex structures generated by the turbulence. It can be approximated best a grid size dependent diffusion coefficient, as originally proposed by Smagorinsky, which lies at the basis of Large Eddy Simulation (LES) (Rodi *et al.*, 2013) . In our case, LES will only be applied to the horizontal diffusion, while the vertical mixing coefficient will be computed from the k-epsilon turbulence model.

4.4 External contributions

External contributions refer to forces and water influxes that influence the North Sea hydrodynamics. These contributions are :

- astral forces that generate tides,
- impact of the Earth's rotation through centrifugal force and the Coriolis force,
- atmospheric conditions (wind, pressure, temperature, rain, evaporation, humidity, cloud cover),

- incoming fresh water.

The following paragraph introduces options available in TELEMAC-3D to activate and simulate these external contributions. More details can be found in the TELEMAC-3D User Manual (2023), in Hervouet (2007) and in the TELEMAC-3D Theory Guide (2023).

Astral forces

Tides are very long waves that move across the ocean and drive the large-scale water level dynamic. They are caused by the gravitational forces exerted by the Moon and the Sun on the Earth and by the inertial force due to the coupled Moon-Earth system rotation.

Mechanics of tide generation and tide propagation then appears of high importance in the processes governing the global ocean flows, and must be carefully considered in modelling processes.

In addition, the English Channel is recognized for hosting *"some of the strongest and most complex tides in the World"* according to Renault & Marchesiello (2022). Then, rendering the tide mechanics occurring within the English Channel and neighborhood regions may provide significant driving conditions to simulate the North Sea hydrodynamic.

TELEMAC-3D is able to generate tides from astral forces. To do so, the logical keyword TIDE GENERATING FORCE needs to be activated and the user must pay attention to adapt the keywords LONGITUDE OF ORIGIN POINT, ORIGINAL DATE OF TIME and ORIGINAL HOUR OF TIME according to the region longitude, and the starting date and hour of the computation.

Earth's rotation

A moving fluid particle on the Earth's surface is subjected to the centrifugal force and the Coriolis force. The centrifugal force concerns fixed and moving fluid particles relatively to the Earth's rotation, whereas the Coriolis force concerns only fluid particles moving relatively to the rotating Earth (Wells, 2012).

These forces are considered as source terms of the momentum balance equations written in spherical coordinates. The centrifugal force is not explicitly added to the momentum equations in the TELEMAC-3D solver, as the latter contribution is found in the *apparent gravity* vector (Hervouet, 2007; Wells, 2012). Besides, the contribution of the vertical velocity in the Coriolis force is ignored in the solver, because it is considered negligible compared to the gravity impact for usual TELEMAC-3D applications. But it may be important in oceanic flows on the mesoscale (Hervouet, 2007). This assumption is then particularly kept in mind for the 3D North Sea model in process.

Finally, the Coriolis force is activated in the solver by setting the logical keyword CORIOLIS to YES and defining the value of the Coriolis coefficient (via the keyword CORIOLIS COEFFICIENT) according to the formulation provided in the TELEMAC-3D User Manual (2023).

4.5 Boundary & Initial conditions

Open sea boundary conditions

TELEMAC-3D offers the possibility to consider open boundaries without forcing any hydrodynamic field; in other words, without prescribing water depth or velocity at fluid boundaries. This option requires the use the *Thompson method,* based on the theory of characteristics (Hervouet, 2007), and will be applied for boundaries open on the Atlantic Ocean and on the Baltic Sea (Figure 4.6).

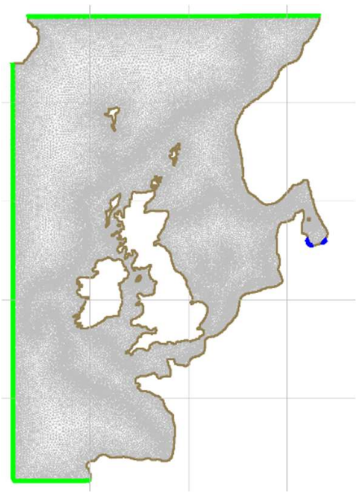

Figure 4.6 Fluid boundaries open on the Atlantic Ocean (green) and on the Baltic Sea (blue)

Land boundary

The water velocity at the land boundary nodes is defined with a slip condition (i.e. direction parallel to the shore), since the mesh resolution cannot take into account the true velocity gradient at solid boundaries.

Incoming fresh water

TELEMAC-3D offers the possibility to place momentum sources in any point of the fluid domain. The horizontal locations of sources are defined with the keyword GLOBAL NUMBERS OF SOURCES, or with the couple of keyword {ABSCISSAE OF SOURCES ; ORDINATES OF SOURCES}. The vertical locations are defined with the keyword ELEVATIONS OF SOURCES.

At each source, the user specifies the liquid flow rate in m^3/s via the keyword WATER DISCHARGE OF SOURCES. In case of sources with variable features, the user can program the USER_T3D_DEBSCE subroutine or call a source file which name is referred in the steering file via the keyword SOURCE FILE.

Atmospheric conditions

Exchanges between water and atmosphere are considered in TELEMAC-3D through the following processes: wind inducing drift of water bodies, solar radiation, atmospheric radiation, water radiation, latent heat due to evaporation and sensitive heat of conductive origin.

These processes simulations require meteorological data the user must gather in the ASCII ATMOSPHERIC DATA FILE of the TELEMAC-3D steering file. These data are: wind magnitude and direction, atmospheric temperature, atmospheric pressure, relative humidity, nebulosity and rainfall. The wind effect can be managed with constant values in space and time with the keyword OPTION FOR WIND.

Initial conditions

As diffusive processes in the deep Atlantic region take thousands of years to reach an equilibrium, the computation initialization from a homogeneous isopycnal state could numerically be out of reach (Haidvogel and Beckmann, 1999). Initializations of computations then require temperature and salinity data close to the realistic instantaneous state of the whole fluid domain of interest. Examples of reanalysis products available online are introduced in Ivanov *et al.* (2020) or Pätsch *et al.* (2017) and mentioned in paragraph 5.5.

Practically, it is recommended to start with a given water surface from an online database (like TPXO). Usually, one has not available the corresponding 3D flow field. Therefore, one typically will start with conditions that do not match the balance of the equations, resulting in errors (and apparent shock waves) that have to dissipate in due time during the first simulated days. By experience, it is known that this so-called “warming-up” of the model takes of the order of one spring-neap cycle (i.e. 14 days). One should try to make sure that initial and boundary conditions are compatible.
For particles, this warming-up period even reaches up to three months before computed particle concentrations may be compared with measured values.

5 North Sea Model Data Sources

Databases sources and respective treatment procedures currently accessible for computation set-up or validation are described in following paragraphs.

5.1 Bathymetry

Bathymetry data are value series that are related to the spatial grid that feed the TELEMAC 3D computations.

These data for the North Sea come from the **EMODnet** database which provides a service for viewing and downloading the best available harmonised Digital Terrain Model (DTM) for the European sea regions through https://emodnet.ec.europa.eu/.

The DTM is generated and regularly updated by the EMODnet Bathymetry partnership using an increasing number of bathymetric data sets. These data are treated and converted via the open-source Geographic Information System **QGIS** and then used in **BlueKenue** for meshing procedure.

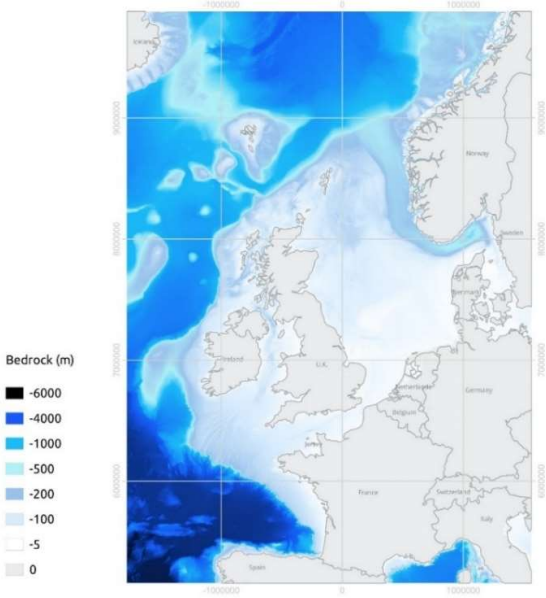

Figure 5.1 Bathymetry of the fluid domain of interest

5.2 Wind and atmospheric pressure

The climate conditions at the water-atmosphere interface will be defined with a 10-meter wind velocity and pressure fields coming from the **ERA-5** database (Hersbach *et al.*, 2020).

In Telemac, the wind stress is modelled as a source term **F** in the momentum equation

$$\boldsymbol{F} = \frac{1}{h}\frac{\rho_{air}}{\rho_{water}} a_{wind}\, \boldsymbol{U_{wind}}\, ||\boldsymbol{U_{wind}}|| \qquad (5.1)$$

$\boldsymbol{U_{wind}}$ is the wind velocity vector coming from the database, ρ_{air} is the volumetric mass of air, ρ_{water} is the volumetric mass of water and a_{wind} is the coefficient of wind influence (Hervouet, 2007).

In the Belgian coastal zone, the impact of wind stress on currents is recognized to be more significant than the local atmospheric pressure gradient (Ruddick and Lacroix, 2006): computation analysis of atmospheric gradient impact on currents will be conducted to attest or not if this observation is valid over the entire North Sea.

Specific attention could be paid to the atmospheric offshore wind farms wakes which impacts on the vertical and lateral flow of the North Sea, which has been recognized strong enough to influence the residual currents and entail alterations of the temperature and salinity distribution (Christiansen *et al.*, 2022). Furthermore, the wind speed at 10 m height is reduced by about 10% in the wind farm area due to the energy extraction induced by the turbine's cascades on the atmospheric flow (Christiansen and Hasager, 2005; Djath *et al.*, 2018).

5.3 Water levels

Water levels data are value series that may be prescribed at the fluid domain boundaries of TELEMAC 3D hydrodynamic computations if the astronomic gravitational fields available in the solver are not able to generate the expected global tide fluctuations.

These data are available in the **TPXO9 database** at https://www.tpxo.net/global/tpxo9-atlas. The changes in water levels may be treated as harmonic oscillating waves and evaluated in the way that it follows the tidal cycle.

5.4 Freshwater inlets

Freshwater inlets are value series that feeds the TELEMAC 3D computations as source terms of the momentum equations and conditions for the salinity and temperature transport treatments.

At the whole North Sea scale, the major haline stratification is localised between the western marine inflows coming from North Atlantic and the eastern fresher inflows coming from the continental coast rivers and the Baltic Sea. Observational data sets based on hydrographic measurements of the North Sea salinity between 1890 and 2011 are available on the **KLIWAS** North Sea database via the web page www.icdc.zmaw.de/knsc_hydrographic.html (Bersch *et al.*, 2013) ; and scalar map of these data on Figure 5.2 provides a global insight of the eastern freshwater contribution in the surface salinity distribution of the North Sea (Pätsch *et al.*, 2017).

All other things, incoming freshwater from the southern rivers seems having a moderate contribution on the whole North Sea salinity distribution. For instance, the major contribution of southern rivers in the total water masses of the Belgian coastal zone has been estimated about 1.9 % for the Rhine/Meuse River, 1.3% for the Scheldt River and 0.8 % for the Seine River (Ruddick and Lacroix, 2006).

Daily freshwater discharges are available on the **Centre for Environmental Prediction (CEFAS, Britain)** for more than 190 rivers bordering the North Sea (Pätsch *et al.*, 2017).

5.5 Salinity and Temperature

Salinity and Temperature data are value series that may be used to : 1) define the flow state at the beginning of a computation , 2) validate the simulation of these scalars transport and distribution.

These data are available on the **KALIWAS** North Sea climatological database, providing hydrographic measurements of salinity and temperature between 1890 and 2011 within 47° to 65°N and 15°W to 15°E frame. Data are found at www.icdc.zmaw.de/knsc_hydrographic.html (Bersch *et al.*, 2013).

These data attests quality controls : they've been monthly and yearly averaged over cells of 0.25° x 0.5° size over 179 levels between 0 and 5000 m depth, thanks to polynomial regressions to remove both monthly and annual cycle trends. A detail description of these data treatments procedures is given by Bersch *et al.* (2013). This database has been used in Pätsch *et al.* (2017) for which uncertainties over averaged salinity and temperature have been estimated small compared to their respective gradient quantities : about 0.027 for salinity and about 0.006°C for temperature. Figure 5.2 depicts scalar maps of these data extracted from Pätsch *et al.* (2017) publication.

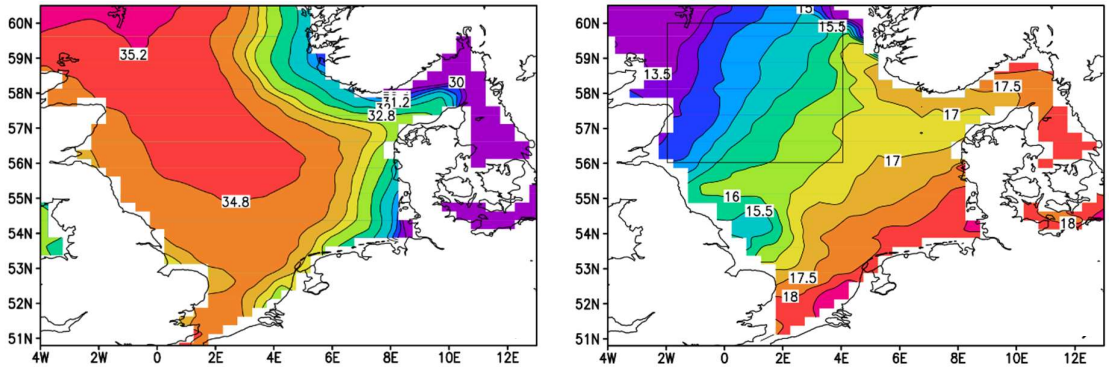

Figure 5.2 Averaged surface salinity distribution a) and surface temperature in August b) coming from the KLIWAS North Sea climatological database (Bersh *et al.*, 2013) and treated between 1998 and 2009 by Pätsch *et al.* (2017). Map a) provides a first insight of the fresher water inlets coming from the eastern continental coast rivers and the Baltic Sea, and their potential contributions over the global North Sea surface salinity.

Data may also be observed from the **Copernicus Marine Service** database, available via the web page https://data.marine.copernicus.eu

5.6 Velocity

Usually, the hydrodynamics is only calibrated to obtain correct water levels. However, this does not guarantee that the velocities are correctly reproduced. Velocity data are thus additional value time series that may be used to calibrate and validate the hydrodynamic results of TELEMAC-3D computations. Such time series are not often available, which explains why this validation is rarely carried out.

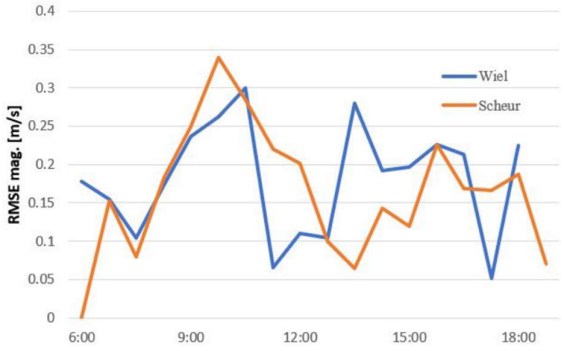

Figure 5.3 Root mean square error of velocity magnitude treated and analysed by Eskens (2021)

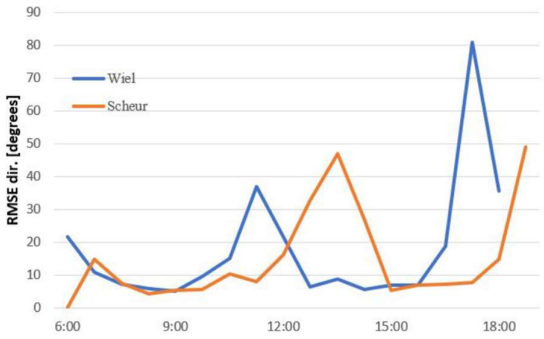

Figure 5.4 Root mean square error of velocity direction treated and analysed by Eskens (2021)

Along the Belgian coast a few useful data sets are available. Two campaigns of velocities measured by an Acoustic Doppler Current Profiler (ADCP) were conducted at Zeebrugge during the summer of 2008. Along a track of approximately 3km, the current velocity is measured by the ADCP at the navigation channels of Scheur and Wielingen. The root mean square error (RSME) of both ADCP measurements has been plotted on Figures 5.3 and 5.4 for velocity magnitude and direction (Eskens, 2021).

There are also data available from a long-term continuous deployment of an acoustic Doppler velocitymeter (ADV) on a bottom mounted tripod offshore near the Port of Zeebrugge (Belgium), managed by the Royal Belgian Institute of Natural Sciences (RBINS, Brussels) (Fettweis *et al.*, 2012).

5.7 Plastics

Plastic concentrations

The available data on plastic concentrations in the North Sea remains very limited in amount and is very scatter in space and time. Moreover, from the field data gathered with the framework of WP2 of the current LABPLAS project, as well as the Flemish PLUXIN project (www.PLUXIN.be) , it is known that variance on the data is two to three time the average value in the rare cases of multiple (i.e. only three) samples taken the same campaign at the same location.

The only other data source is the EMODnet data base on macro litter (mainly plastic bags) collected in trawling fishing, i.e. giving an indication of plastic accumulations on the sea floor. This dataset was used by IMDC as a testcsae for their preliminary North Sea plastic litter dispersal model (Eskens, 2021).

We propose to apply the approach adopted in the PLUXIN project (Shettigar & Toorman, 2024) to initiate the model with an estimated amount (total mass) of plastics in the domain and let the model run to obtain a quasi-equilibrium distribution. This concentration field subsequently is taken as the background concentration, to be validated with the scarce field data, after rescaling (i.e. a data assimilation step will be conducted). The resulting model should then be ready to be used for scenario analyses.

Plastic inlet sources

The estimation of plastic litter inlets from rivers is of high importance to simulate their propagation through the North Sea. This data is treated as a source term in the plastic particles transport equation of the solver.

The income of mismanaged plastic waste is estimated by Eskens (2021). The data on the river catchment is taken from the European Catchment and Rivers network system of the European Environmental Agency through the web page https://www.eea.europa.eu/data-and-maps/data/european-catchments-and-rivers-networks.

Eskens (2021) quantify the mass of mismanaged plastic waste (M_{MSW}) for countries various European countries and is depicted in Figure 5.5, where the rivers basins are sorted as the highest plastic production.

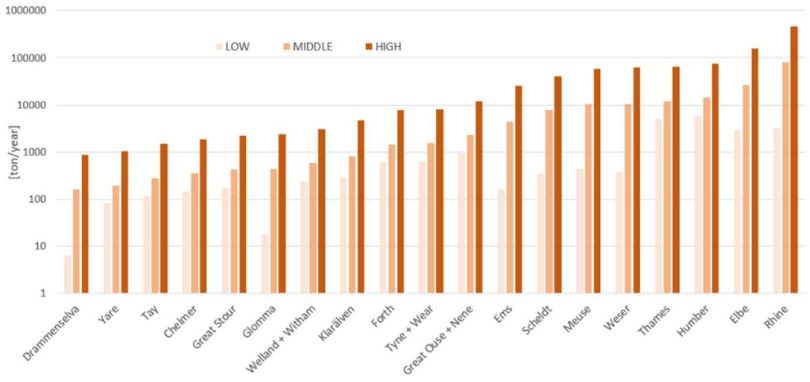

Figure 5.5 River basins sorted as the highest plastic production

Furthermore, the estimation of mass of plastic that is released at North Sea river mouths requires the river surface and subsurface runoff values, which series are found in the databases of the Global Land Data Assimilation System available from

https://disc.gsfc.nasa.gov/datasets?keywords=GLDAS.

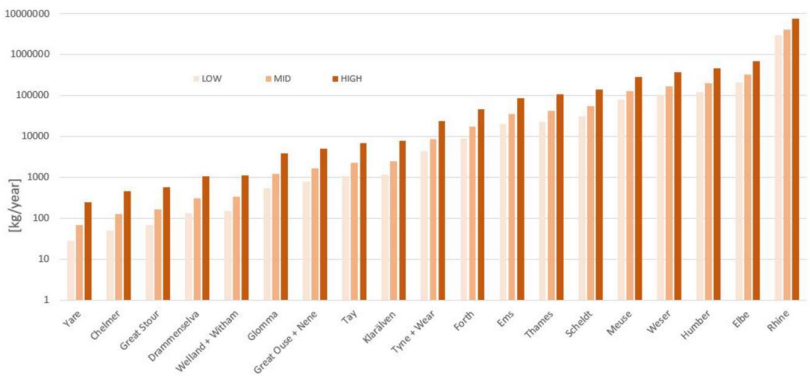

Figure 5.6 Mass of plastic output of major rivers per year

From the above quantities, the total mass of plastic output a river per day can be estimated. Figure 5.6 provides an insight of results available per year for major rivers bordering the North Sea (Eskens, 2021).

However, this classical approach is not in agreement with observations and measurements in the field. Evidence from recent campaigns in the Elbe (Germany) (Scherer *et al.*, 2020; www.LAPBPLAS.eu) and Scheldt (Belgium) (Shettigar & Toorman, 2024; www.PLUXIN.be) strongly suggests that much of the plastic flux towards the sea gets trapped in intertidal areas, on the shore, and in the sediment bed, in particular within the estuarine part of the river. Therefore, one has to correct the above values with an "estuarine retention" factor. The determination of this correction factor is expected to depend on the shape (and asymmetry) of the tidal signal over one tide.

5.8 Sediment

The model requires sediment data both for initialisation and boundary conditions of the sediment transport model. Also, additional datasets are required to validate the model. The sediment transport model requires datasets such as the grain size distribution (GSD), bed layer thicknesses and suspended sediment concentrations. These often collected and reported at low spatial and temporal resolution owing to the intensive field campaign requirements. Therefore alternative (proxy) measurement values are often proposed, such as remote sensing turbidity or colour values as a proxy for suspended sediment concentrations. Bed layer thickness values are often not available at large spatial scales. Therefore model is initialised with assumed uniform thickness values for bed layer thickness and the bedload transport model determines the bed layer thicknesses.

The GSD is used to determine the median sediment size and mud to sand ratio which are required for the sediment transport model. However, a full GSD is almost never available in the full expanse

of the model domain. Several regional organisations collect the GSD data at different time scales using different methodologies. EMODnet Geology portal[4] provides with a harmonized dataset which is derived from several regional dataset. The data of the seabed substrate is provided in Folk classification system of 5, 7 and 16 classes. This cover all of the European maritime areas in one product. With such a classification, rough estimates of GSD can be made. Further, mud to sand ratio can be derived.

Similarly, the suspended sediment concentration (SSC) is not available at full expanse of the model domain. It is measured by the regional entities, usually in the territorial waters. However for the North-Sea model application, data needs to be available in much larger spatial extent. Often, satellite imagery are utilised to overcome the lack of SSC data (Gayer et al., 2006; Knaeps et al., 2017). Remote sensing instruments aboard satellites capture electromagnetic radiation reflected or emitted from the Earth's surface. Different wavelengths can be used to detect different features, including SSC. Suspended sediment affects the reflectance properties of water. Particles in the water column scatter and absorb light, altering the spectral signature of the water body. By analysing these changes in reflectance, inferences can be drawn on presence and concentration of suspended sediment. To estimate SSC accurately, satellite imagery needs to be calibrated and validated using ground-based measurements. This involves collecting water samples at various locations and times to determine actual sediment concentrations. Despite its advantages, satellite-based estimation of SSC also faces challenges, such as atmospheric interference, cloud cover, and limitations in sensor capabilities. Additionally, factors like water turbidity, bottom reflectance, and variations in sediment composition can affect the accuracy of SSC estimates.

[4] https://emodnet.ec.europa.eu/geoviewer/

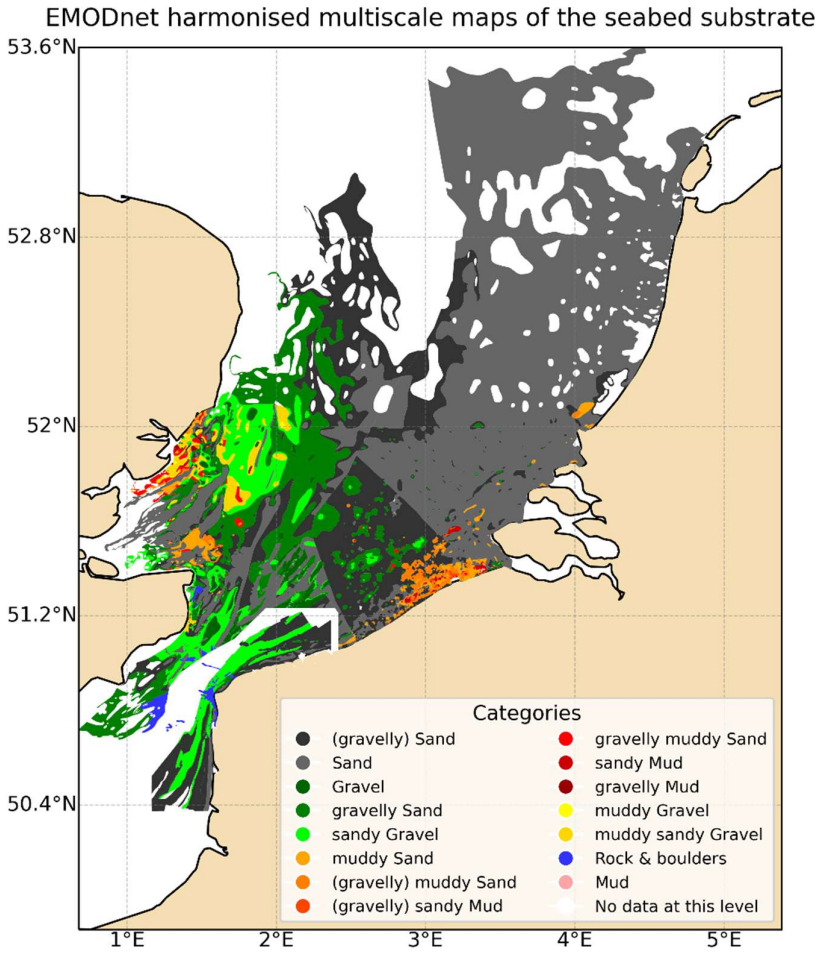

Figure 5.7 The EMODnet Folk 16 classification of the seabed substrate over the expanse of Southern North-sea.

6 REFERENCES

Breugem, W., E. Fonias, L.Wang, A. Bolle, G. Kolokythas, and B. De Maerschalck (2019).Tel2tom: coupling telemac2d and tomawac on arbitrary meshes. In: XXVIth TELEMAC-MASCARET User Conference (15-17 Oct.2019, Toulouse, 2019.

Cheng N.S. (1997). *Simplified settling velocity formula for sediment particle*. J. of Hydraulic Engineering ASCE, 123(2):149-152.

Kramer O.J.I., de Moel P.J., Raaghav S.K.R., Baars E.T., van Vugt W.H., Breugem W.-P., Padding J.T., van der Hoek J. P. (2021). *Can terminal settling velocity and drag of natural particles in water ever be predicted accurately?*. Drink. Water Eng. Sci., 14, 53–71.

Pedrotti, M.L., Labis, E., Riom, W., Shettigar, N., Toorman, E.A. (2023). Technical report describing the multi-parameter settling velocity closure - Deliverable 7.8, LABPLAS Grant Agreement No. 101003954 H2020-SC5-2020-2.

Andersen, T.J., Rominikan, S., Olsen, I.S., Skinnebach, K.H., Fruergaard, M. (2021). Flocculation of PVC microplastic and fine-grained cohesive sediment at environmentally realistic concentrations. The Biological Bulletin, 240(1), 42-51.

Baba, J., Komar, P.D. (1981). Measurements and analysis of settling velocities of natural quartz sand grains. J. Sediment. Petrol., 51, 631– 640.

Benoit M., Marcos F., Becq F. (1996). Development of a third generation shallow water wave model with unstructured spatial meshing. Proc. 25th Int. Conf. on Coastal Eng. (ICCE'1996, 2-6 September 1996, Orlando, Florida, USA), pp 465-478.Bersch, M., Gouretski, V., Sadikini, R., Hinrichs, I., 2013. *Hydrographic climatology of the North Sea and surrounding regions.* Centre for Earth System Research and Sustainability, University of Hamburg. www.icdc.zmaw.de/knsc_hydrographic.html

Briggs, L., McCulloch, D., Moser, F. (1962). The hydraulic shape of sand particles. J. Sediment. Petrol., 32(4), 645–656.

Camenen B. (2007). Simple and general formula for the settling velocity of particles. J. Hydraul. Eng., 133(2): 229-233.

Characklis, W.G. (1991). Biofouling: effects and control. In Biofouling and Biocorrosion in Industrial Water Systems: Proceedings of the International Workshop on Industrial Biofouling and Biocorrosion, Stuttgart, September 13–14, 1990 (pp. 7-27). Springer Berlin Heidelberg.

Cheng, N.S. (1997). Simplified settling velocity formula for sediment particle. J. Hydr. Eng., 123(2):149-152.

Christiansen N, Daewel U, Djath B and Schrum C (2022) *Emergence of Large-Scale Hydrodynamic Structures Due to Atmospheric Offshore Wind Farm Wakes.* Front. Mar. Sci. 9:818501. Doi: 10.3389/fmars.2022.818501

Christiansen, M. B., and Hasager, C. B. (2005). *Wake effects of large offshore wind farms identified from satellite SAR*. Remote Sens. Env. 98, 251-268. Doi: 10.1016/j.rse.2005.07.009

Clift, R., Gauvin, W.H. (1970). The motion of particles in turbulent gas streams. Proc. Chemeca '70, Australian National Committee of the Institution of Chemical Engineers and the Australian Academy of Science (Melbourne and Sydney, Australia, August 1970).

Corey A.T. (1949). Influence of shape on the fall velocity of sand grains. PhD thesis, Colorado State University, Fort Collins, CO.

Dallavalle, J. (1948). Micrometrics: The Technology of Fine Particles, Pitman, London.

Dietrich, W. E. (1982). Settling velocity of natural particles. Water Resources Research, 18(6), 1615-1626.

Digouardi F., Mele D. (2015). A new shape dependent drag correlation formula for non-spherical rough particles. Experiments and results. Powder Technology, 277.

Digouardi F., Mele D., Dellino P. (2018). A new one-equation model of fluid drag for irregularly shaped particles valid over a wide range of Reynolds number. J. Geophysical Research: Solid Earth, 123, 144–156.

Djath, B., Schulz-Stellenfleth, J., and Canadillas, B. (2018). *Impact of atmospheric stability on X-band and C-band synthetic aperture radar imagery of offshore windpark wakes.* J. Renew. Sust. Energy 10:43301. Doi: 10.1063/1.5020437

Escobar, S., Bi, Q., Fettweis, M., Wongsoredjo, S., Monbaliu, J., Toorman, E. (2023). A dynamic 2DH flocculation model for coastal domains. Ocean Dynamics (in press).

Esteban, L.B., Shrimpton, J.S., Ganapathisubramani, B. (2020). Disks settling in turbulence. J. Fluid Mechanics, 883, A58.

Eskens, L. (2021), *Hydraulic transport of Marine Plastics in the North Sea – Exploratory Research*. Master of Science Thesis, KU Leuven, 2021.

Fazey, F.M., Ryan, P.G. (2016). Biofouling on buoyant marine plastics: An experimental study into the effect of size on surface longevity. Environmental Pollution, 210, 354-360.

Fettweis, M., Baeye, M., Lee, B., Chen, P., Yu, J. (2012) Hydro-meteorological influences and multimodal suspended particle size distributions in the Belgian nearshore area (southern North Sea). Geo-Marine Letters, 32(2), 123–137.

Fischer, R., Lobelle, D., Kooi, M., Koelmans, A., Onink, V., Laufkötter, C., ... van Sebille, E. (2022). Modelling submerged biofouled microplastics and their vertical trajectories. Biogeosciences, 19(8), 2211-2234.

Gall, S.C., Thompson, R.C. (2015). The impact of debris on marine life. Marine Pollution Bulletin, 92(1-2), 170-179.

Gayer, G., Dick, S., Pleskachevsky, A., & Rosenthal, W. (2006). Numerical modeling of suspended matter transport in the North Sea. *Ocean Dynamics*, *56*(1), 62–77. https://doi.org/10.1007/S10236-006-0070-5/FIGURES/12

GESAMP (2015) Sources, fate and effects of microplastics in the marine environment: a global assessment. Kershaw PJ (ed). Rep Stud GESAMP No. 90, 96 pp

Geyer, R., Jambeck, J.R., Law, K.L. (2017). Production, use, and fate of all plastics ever made. Science Advances, 3(7), e1700782.

Haider, A., Levenspiel, O. (1989). Drag coefficient and terminal velocity of spherical and nonspherical particles. Powder Technology, 58(1), 63-70.

Haidvogel, D. B., Beckmann, A., *Numerical Ocean Circulation Modeling*, Published in 1999 by Imperial College Press. ISBN 1-86094-114-1

Hallermeier R. (1981). Terminal settling velocity of commonly occurring sand grains. Sedimentology, 28(6), 859-865.

Hasselmann, K.; Barnett, T.P.; Bouws, E.; Carlson, H.; Cartwright, D.E., Enke, K. Ewing, J.A. Gienapp, H.;, Hasselmann, D.E., Kruseman, P.; Meerburg, A.; Muller, P.; Olbers, D.J.; Richter, K.; Sell, W.; Walden, H. (1973). Measurements of wind-wave growth and swell decay during the joint north sea wave project (jonswap). Deutschen Hydrographischen Zeitschrift, 8 N 12.

Hersbach, H., Bell, B., Berrisford, P., Hirahara, S., Horanyi, A., Munoz-Sabater, J., Nicolas, J., Peubey, C., Radu, R., Schepers, D. *et al. The era5 global reanalysis.* Quarterly Journal of the Royal Meteorological Society, 146(730):1999-2049, 2020.

Hervouet J.-M., *Hydrodynamics of Free Surface Flows: Modelling with the finite element method,* 2007 John Wiley & Sons Edition, Ltd. ISBN: 978-0-470-03558-0

Hoerner S.F. (1965). Fluid Dynamic Drag. Bakersfield (CA): Hoerner Fluid Dynamics.

Holthuijsen L. H. (2007). Waves in Oceanic and Coastal Waters. Cambridge University Press

Hölzer A., Sommerfeld M. (2008). New simple correlation formula for the drag coefficient of non-spherical particles. Powder Technology 184, 361-365.

Knaeps, E., Sterckx, S., Bhatia, N., Bi, Q., Monbaliu, J., Toorman, E., Cattrrijsse, A., Keukelaere, L. De, & Abstract. (2017). COASTAL TURBIDITY MONITORING USING THE PROBA-V SATELLITE. *Coastal Dynamics*, 1483–1494.

ISO, P. (2019). 1183-1; Plastics—Methods for Determining the Density of Non-Cellular Plastics—Part 1: Immersion Method, Liquid Pycnometer Method and Titration Method. PKN: Płock, Poland.

Ivanov, E., Capet, A., Barth, A., Delhez, E. J.M., Soetaert, K., Grégoire, M., *Hydrodynamic variability in the Southern Bight of the North Sea in response to typical atmospheric and tidal regimes. Benefit of using a high resolution model*, Ocean Modelling 154 (2020) 101682

Joly A., Goeury C., Hervouet J.-M., *Adding a particle module to Telemac-2D with applications to algae blooms and oils spills.* Technical Report H-P74-2013-02317-EN, EDF R&D-LNHE, 2013.

Jalón-Rojas, I., Romero-Ramírez, A., Fauquembergue, K., Rossignol, L., Cachot, J., Sous, D., Morin, B. (2022). Effects of biofilms and particle physical properties on the rising and settling velocities of microplastic fibers and sheets. Env. Science & Technology.

Jambeck, J.R. *et al.* (2015). Plastic waste inputs from land into the ocean. Science, 347, 768–771.

Janke N.C. (1966). *Effect of shape upon the settling velocity of regular convex geometric particles*. J. Sedimentary Petrology, 36(2), 370-376.

Julien, P. (1995). Erosion and sedimentation, Cambridge University Press, Cambridge, U.K.

Kaiser, D., Kowalski, N., Waniek, J.J. (2017). Effects of biofouling on the sinking behavior of microplastics. Env. Research Letters, 12(12), 124003.

Kaskas A. (1964). Berechnung der stationären und instationären Bewegung von Kugeln in ruhenden und strömende Medien. Dipl. Thermodynamik und Verfahrenstechnik, TU Berlin.

Khatmullina, L., Isachenko, I. (2017). Settling velocity of microplastic particles of regular shapes. Mar. Pollut. Bull, 114, 871−880.

Klonaris, G.; Van Eeden, F.; Verbeurgt, J.; Troch, P. ; Constales, D.; Poppe, H. ; De Wulf, A., *ROMS Based Hydrodynamic Modelling Focusing on the Belgian Part of the Southern North Sea,* J. Mar. Sci. Eng. **2021**, 9, 58. https://doi.org/10.3390/jmse9010058

Kooi, M., Nes, E.H.V., Scheffer, M., Koelmans, A.A. (2017). Ups and downs in the ocean: effects of biofouling on vertical transport of microplastics. Env. Science & Technology, 51(14), 7963-7971.

Kowalski, N., Reichardt, A.M., Waniek, J.J. (2016). Sinking rates of microplastics and potential implications of their alteration by physical, biological, and chemical factors. Mar. Pollut. Bull., 109, 310−319.

Kreczak, H., Willmott, A.J., Baggaley, A.W. (2021). Subsurface dynamics of buoyant micro-plastics subject to algal biofouling. Limnology and Oceanography, 66(9), 3287-3299.

Krumbein W.C. (1941). Measurement and geological significance of shape and roundness of sedimentary particles. J. Sedimentary Petrology, 11: 64-72.

Laursen, S.N., Fruergaard, M., Andersen, T.J. (2022). Rapid flocculation and settling of positively buoyant microplastic and fine-grained sediment in natural seawater. Marine Pollution Bulletin, 178, 113619.

Leith, D. (1987). Drag on nonspherical objects. Aerosol Sci. Tech., 6, 153-161.

Leiser, R., Schumann, M., Dadi, T., Wendt-Potthoff, K. (2021). Burial of microplastics in fresh-water sediments facilitated by iron-organo flocs. Scientific Reports, 11(1), 1-12.

Li, B., Zhao, J., Ge, W., Li, W., Yuan, H. (2022). Coagulation-flocculation performance and floc properties for microplastics removal by magnesium hydroxide and PAM. J. Env. Chem. Eng., 10(2), 107263.

Li, Y., Wang, X., Fu, W., Xia, X., Liu, C., Min, J., ... Crittenden, J. C. (2019). Interactions between nano/micro plastics and suspended sediment in water: Implications on aggregation and settling. Water Research, 161, 486-495.

Lobelle, D., Kooi, M., Koelmans, A. A., Laufkötter, C., Jongedijk, C. E., Kehl, C., van Sebille, E. (2021). Global modeled sinking characteristics of biofouled microplastic. J.Geophysical Research: Oceans, 126(4), e2020JC017098.

Lusher, A. (2015). Microplastics in the marine environment: distribution, interactions and effects. Marine Anthropogenic Litter, 245-307.

GMR Plastics Europe, Conversion Market & Strategy GmbH. Plastics—The Facts 2019.

Mei, R. (1994). Effect of turbulence on the particle settling velocity in the nonlinear drag range. Int. J. Multiphase Flow, 20(2), 273-284.

Mendrik, F., Fernández, R., Hackney, C.R., Waller, C., Parsons, D.R. (2023). Non-buoyant micro-plastic settling velocity varies with biofilm growth and ambient water salinity. Communications Earth & Environment, 4(1), 30.

Miao, L., Gao, Y., Adyel, T. M., Huo, Z., Liu, Z., Wu, J., Hou, J. (2021). Effects of biofilm colonization on the sinking of microplastics in three freshwater environments. J. Hazardous Materials, 413, 125370.

Pätsch J., Burchard H., Dieterich C., Gräwe U., Gröger M., Mathis M., Kapitza H., Bersch M., Moll A., Pohlmann T., Su J., Ho-Hagemann H. T.M., Schulz A., Elizalde A., Eden C. *An evaluation of the North Sea circulation in global and regional models relevant for ecosystem simulations*, Ocean Modelling 116 (2017) 70-95.

Potthoff, A., Oelschlägel, K., Schmitt-Jansen, M., Rummel, C.D., Kühnel, D. (2017). From the sea to the laboratory: Characterization of microplastic as prerequisite for the assessment of ecotoxicological impact. Integrated Environmental Assessment and Management, 13(3), 500-504.

Renault, L., Marchesiello, P., (2022) *Ocean tides can drag the atmosphere and cause tidal winds over broad continental shelves*, Communications Earth & Environment, DOI : https://doi.org/10.1038/s43247-022-00403-y

Revil-Baudard, T., Akutina, Y., Eiff, O. (2017). Settling velocity in a turbulence column and its effect on the suspension profile. EGU General Assembly Conference Abstracts (p. 2238).

Richardson J.F., Zaki W.N. (1954). Sedimentation and fluidisation: Part I. Trans. Inst. Chem. Eng., 32, 35–53.

Riom, W., Shettigar, N.A., Toorman, E. (2022). Process based model for riverine plastic fluxes. *Proc. XXVIIIth TELEMAC User Conference* (18-19 October 2022, Paris-Saclay), pp.247-253.

Ruddick K. and Lacroix G., *CHAPTER 1: Hydrodynamic and meteorology of the Belgian Costal Zone*, Published in "Current status of eutrophication in the Belgian Coastal Zone" By V. Rousseau, C. Lancelot and D. Cox (eds), Presses Universitaires de Bruxelles, 2006, Copyright BELSPO.

Rochman CM, Browne MA, Underwood AJ, van Franeker JA, Thompson RC, Amaral-Zettler LA (2016). The ecological impacts of marine debris: unraveling the demonstrated evidence from what is perceived. Ecology 97: 302-312.

Rodi, W., Constantinescu, G., Stoesser, T. (2013). Large-Eddy Simulation in Hydraulics. London: CRC Press, 266 pp.

Scherer, C. *et al.* (2020). Comparative assessment of microplastics in water and sediment of a large European river. Sci. Total. Environ. 738, 139866.

Schiller, L., Naumann, A. (1933). Über die grundlegenden Berechnungen bei der Schwerkraft-aufbereitung. Z. Ver. Deutsch. Ing. 77, 318-320.

Shettigar, N.A., Toorman, E. (2024). Development of two-dimensional horizontal plastic dispersal model, model validation and uncertainty assessment. PLUXIN project Deliverable D3.1, D3.2, D3.3, D3.4 and D3.5, Hydraulics & Geotechnics, KU Leuven.

Shettigar, N.A., Bi, Q., Toorman, E. (2024). Assimilating the size diversity: Population Balance Equations applied to the modelling of microplastics transport. Environmental Science and Technology (under review).

Soulsby, R. (1997). Dynamics of marine sands, a manual for practical applications, Thomas Telford, London.

Stokes, G.G. (1851). On the effect of the internal friction on the motion of pendulums. Cambridge Phil. Trans., 9: 8-106.

Tassi, P.; Benson, Th.; Delinares, M.; Fontaine, J.; Huybrechts, N.; Kopmann, R.; Pavan, S.; Pham, C.-T.; Taccone, F.; Walther, R. (2023). GAIA - a unified framework for sediment transport and bed evolution in rivers, coastal seas and transitional waters in the TELEMAC-MASCARET modelling system, Environmental Modelling & Software, 59, 105544. https://doi.org/10.1016/j.envsoft.2022.105544.

Toorman E.A. (2002). Modeling of turbulent flow with cohesive sediment. In: Proc. in Marine Science, Vol.5: Fine Sediment Dynamics in the Marine Environment (J.C. Winterwerp & C. Kranenburg, eds.), pp.155-169, Elsevier Science, Amsterdam.

Toorman.E, (2022) Modification of the Dietrich (1982) formula and a new closure for the terminal settling velocity of spherical particles, Internal note, Hydraulics Laboratory, KU Leuven.

Turton R., Clark N.N. (1987). An explicit relationship to predict spherical particle terminal velocity. Powder Technol,, 53, 127-129.

TELEMAC-3D User Manual, Version v8p5, December 1, 2023,

Wadell, H. (1932). Volume, shape, and roundness of rock particles. J. Geology, 40: 443-451.

Waldschläger, K.; Schüttrumpf, H. (2019). Effects of particle properties on the settling and rise velocities of microplastics in freshwater under laboratory conditions. Environ. Sci. Technol, 53, 1958-1966.

Wells, Neil. *The Atmosphere and Ocean : A physical introduction,* Third Edition. Neil C. Wells. 2012 John Wiley & Sons, Lyd. Published 2012 by John Wiley & Sons, Ltd. ISBN 978-0-470-69469-5.

Williams, G. (1966). Particle roundness and surface texture effects on fall velocity. J. Sediment. Petrol., 36(1), 255–259.

Wu, W., Wang, S.S. (2006). Formulas for sediment porosity and settling velocity. J. Hydr. Eng., 132(8), 858-862.

Zhou, Q., Cheng, N.S. (2009). Experimental investigation of single particle settling in turbulence generated by oscillating grid. Chemical Engineering Journal, 149(1-3), 289-300.